THE UNIVERSITY OF WARWICK

Library Declaration and Deposit Agreement

1. **STUDENT DETAILS**

   Amena Faruqi
   2187947

2. **THESIS DEPOSIT**

   2.1 I understand that under my registration at the University, I am required to deposit my thesis with the University in BOTH hard copy and in digital format. The digital version should normally be saved as a single pdf file.

   2.2 The hard copy will be housed in the University Library. The digital version will be deposited in the University's Institutional Repository (WRAP). Unless otherwise indicated (see 2.3 below) this will be made openly accessible on the Internet and will be supplied to the British Library to be made available online via its Electronic Theses Online Service (EThOS) service. [At present, theses submitted for a Master's degree by Research (MA, MSc, LLM, MS or MMedSci) are not being deposited in WRAP and not being made available via EthOS. This may change in future.]

   2.3 In exceptional circumstances, the Chair of the Board of Graduate Studies may grant permission for an embargo to be placed on public access to the hard copy thesis for a limited period. It is also possible to apply separately for an embargo on the digital version. (Further information is available in the Guide to Examinations for Higher Degrees by Research.)

   2.4 (a) Hard Copy I hereby deposit a hard copy of my thesis in the University Library to be made publicly available to readers immediately.
   I agree that my thesis may be photocopied.

   (b) Digital Copy I hereby deposit a digital copy of my thesis to be held in WRAP and made available via EThOS.
   My thesis can be made publicly available online.

3. **GRANTING OF NON-EXCLUSIVE RIGHTS**

   Whether I deposit my Work personally or through an assistant or other agent, I agree to the following: Rights granted to the University of Warwick and the British Library and the user of the thesis through this agreement are non-exclusive. I retain all rights in the thesis in its present version or future versions. I agree that the institutional repository administrators and the British Library or their agents may, without changing content, digitise and migrate the thesis to any medium or format for the purpose of future preservation and accessibility.

4. **DECLARATIONS**

   (a) I DECLARE THAT:

   - I am the author and owner of the copyright in the thesis and/or I have the authority of the authors and owners of the copyright in the thesis to make this agreement. Reproduction of any part of this thesis for teaching or in academic or other forms of publication is subject to the normal limitations on the use of copyrighted materials and to the proper and full acknowledgement of its source.
   - The digital version of the thesis I am supplying is the same version as the final, hardbound copy submitted in completion of my degree, once any minor corrections have been completed.
   - I have exercised reasonable care to ensure that the thesis is original, and does not to the best of my knowledge break any UK law or other Intellectual Property Right, or contain any confidential material.
   - I understand that, through the medium of the Internet, files will be available to automated agents, and may be searched and copied by, for example, text mining and plagiarism detection software.

   (b) IF I HAVE AGREED (in Section 2 above) TO MAKE MY THESIS PUBLICLY AVAILABLE DIGITALLY, I ALSO DECLARE THAT:

   - I grant the University of Warwick and the British Library a licence to make available on the Internet the thesis in digitised format through the Institutional Repository and through the British Library via the EThOS service.
   - If my thesis does include any substantial subsidiary material owned by third-party copyright holders, I have sought and obtained permission to include it in any version of my thesis available in digital format and that this permission encompasses the rights that I have granted to the University of Warwick and to the British Library.

5. **LEGAL INFRINGEMENTS**
   I understand that neither the University of Warwick nor the British Library have any obligation to take legal action on behalf of myself, or other rights holders, in the event of infringement of intellectual property rights, breach of contract or of any other right, in the thesis.

Please sign this agreement and return it to the Graduate School Office when you submit your thesis.

Student's signature: ....Date: 06 September 2022

Simulating the Transit of a Binary System by a Circumbinary Disc in the HD98800 System

by

Amena Faruqi

Thesis

Submitted to the University of Warwick

for the degree of

Master of Science (by Research) in Physics

Department of Physics

September 2022

Contents

List of Tables

List of Figures

Acknowledgments

I would like to take the opportunity to acknowledge and express thanks to Dr Grant Kennedy, Dr Rebecca Nealon, and Dr Sahl Rowther for all of their help in completing this project. Our conversations, ranging from scientific discussions to working together to debug code, were invaluable to me and one of the best educational experiences I have had. The research presented here would not have been possible without their guidance and for that, I am extremely grateful.

I am very grateful for the new friends I have made in the past year. Being a newcomer is always daunting, especially while simultaneously diving headfirst into my first experience with research, but the community spirit of the Warwick Astronomy group has made the experience exponentially easier.

I would also like to thank my family and friends for their support. In spite of not understanding much of my research, they were always happy to hear what I was working on and offer some much-needed opportunities to de-stress. I especially would like to thank my mum for her unwavering support, without which I could not have made it this far. And finally, I would like to acknowledge my grandfather, who always wanted me to pursue a PhD but passed away just months before my acceptance onto a PhD programme. I hope he would have been proud.

Declarations

I declare that the research and results presented in this thesis are my own and have not been submitted to any other academic institution for any other degree or qualification. This research was undertaken at the University of Warwick, during the period from September 2021 to September 2022, under the supervision of Dr Grant Kennedy, Dr Rebecca Nealon, and Dr Sahl Rowther. This research made use of existing software – `Phantom` and `SPLASH`, created by Dr Daniel Price, `MCFOST`, created by Dr Christophe Pinte, and `REBOUND`, created by Dr Hanno Rein and Dr Daniel Tamayo.

Abstract

HD98800 is a quadruple star system consisting of two binaries, AaAb and BaBb, one of which (BaBb) has been observed to have a circumbinary protoplanetary disc encircling it. It has been predicted that in a few years, the circumbinary disc of BaBb will pass in front of AaAb, providing an alternative way to quantify the disc structure. In this project, hydrodynamical simulations and radiative transfer models were used to create synthetic time series observations of the HD98800 system and anticipated transit. In order for the results to be comparable to data from optical telescopes, all synthetic observations were produced at optical wavelengths ($\lambda = 0.8\mu m$). To consider how observations differ as a result of variations in disc properties, a grid of models defined by a parameter space consisting of different values of the disc's dust mass, gas mass, viscosity, and dust grain size was created. These results were then compared to identify features in the synthetic light curves that could be used to make inferences about disc properties and more broadly, how certain disc properties can be constrained using simulation data. The results were then used to provide some recommendations for future observations and subsequent study of the system and transit, as well as providing some insight into the properties of circumbinary protoplanetary discs.

Chapter 1

Introduction

Binary stars are pairs of stars that orbit around a shared centre of mass. Initially thought to be a chance alignments of single stars, it was William Herschel who first coined the term "binary star" in the 1700s to refer to these pairs in his *Catalogue of Double Stars* (Herschel, 1782). After noting that they were observed too frequently to be single stars occasionally aligning, he concluded that these must be bodies that are gravitationally bound, obeying Newton's law of gravitation. Since then, many more binary systems have been detected and imaged, to the point where we now believe the majority of stars are part of binary or higher order multi-star systems (Raghavan et al., 2010), vastly expanding our knowledge of the inventory of the Universe.

Our observations of binary stars have indicated that, much like single stars, accretion discs of gas and dust can form around binary star systems (Kraus et al., 2011), which could serve as sites for the formation of circumbinary planets. The dynamics of these circumbinary systems are dependent on a number of factors – the dust-to-gas ratio, mass and size of the circumbinary discs, as well as torques exerted by the inner stars can lead to the existence of systems with widely varying configurations (Thun et al., 2017). The broad range of physical effects, many of which are unique to multi-star systems, has interesting implications for the formation of stable planetary systems from protoplanetary discs. Given how many binary systems have been found to-date (Gaia Collaboration et al., 2022), and the fact that observations of exoplanetary systems from the Kepler mission have shown that planets can form in the region around binary stars (Doyle et al., 2011), there is ample motivation for further research into circumbinary discs.

This project sets out to further our current understanding of the nature of binary systems and circumbinary discs through the use of computational simulations of a specific system, known as HD98800. Hence, the remainder of this chapter will provide some scientific background and context for the subject of study. In chapter 2, I will provide an overview of the suite of computational techniques and code used, explaining the methodology employed to build and run the simulations, how parameters were chosen and how final outputs based on simulation data were produced. Chapter 3 will contain the results produced from all of the simulations, which can then be compared and discussed to consider what conclusions can be drawn. Additionally, any limitations to my methods and how they may have affected the results will be discussed. In chapter 4, a brief summary of the results will be provided, along with recommendations for observations and future work.

1.1 Binary Star Systems

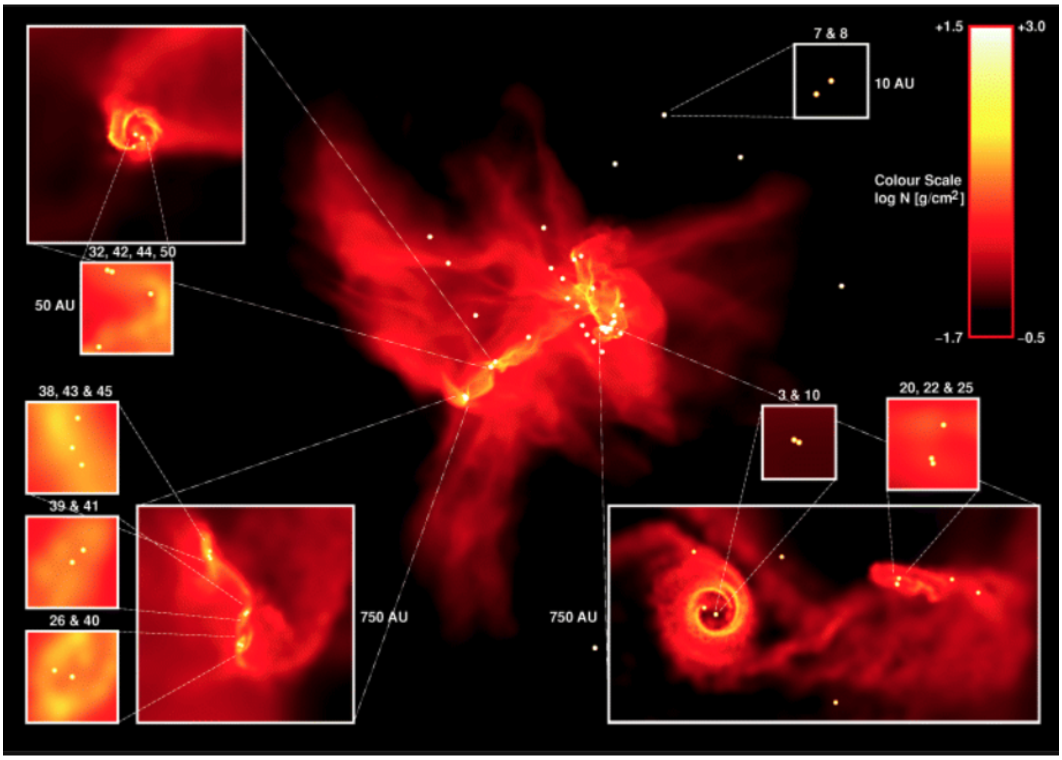

Figure 1.1: Frame from a hydrodynamical simulation by Bate et al. (2002), showing the formation of seven close binaries via disc fragmentation.

Stars are created from rotating molecular cloud cores that undergo collapse under gravity until a protostar is formed in the centre, embedded within a cloud of gas and dust (e.g. Armitage, 2020). To explain how multi-star systems can fit into this picture of star formation, a number of different theories have been explored over the years (e.g. Tohline, 2002; Kratter, 2011). Of these, the two main theories are in agreement that some instability must arise, leading to the fragmentation of either a cloud core prior to the creation of a central protostar or a protostellar disc, allowing for the formation of two or more stars within the same disc. One theory, referred to as "turbulent fragmentation", involves density perturbations caused by turbulence in the cloud core, which can create regions within the core where collapse is accelerated relative to the surrounding material (Goodwin et al., 2004). The second theory, known as the "disc fragmentation" hypothesis, suggests that a protostellar disc around a pressure-supported core can fragment to form protobinaries (Bonnell and Bate, 1994), as seen in fig 1.1. The former offers a more plausible explanation for binaries with separations greater than 500 AU, whereas the latter is better for explaining close binaries (Offner et al., 2010).

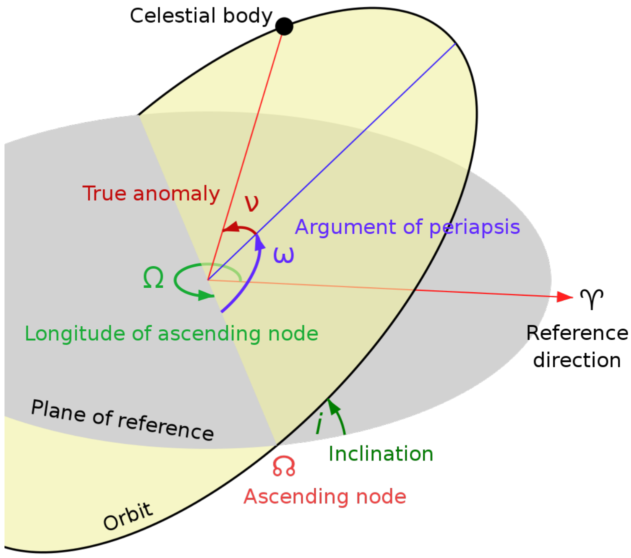

Figure 1.2: Diagram showing the orbital elements of a celestial body. a is the semi-major axis, e is the eccentricity, i is the inclination angle of the orbital plane, Ω is the longitude of ascending node, ω is the argument of periapsis, and ν is the true anomaly (Wikipedia contributors, 2007). For binary systems, the reference plane is typically the sky plane, and North is the reference direction.

Once they have reached a stable state, binary stars will orbit a shared centre of mass. By designating the brighter of the two stars as the "primary" (and consequently, the dimmer as the "secondary"), we can shift into the reference frame of the primary star. Then, binary orbits can be defined in terms of the orbital elements used to define the motion of celestial bodies about a central point (see fig 1.2), where the moving body is the secondary moving relative to the, now fixed, primary. Then, a is the average distance between the primary and secondary (semi-major axis), e is the eccentricity, a measure of how non-circular an orbit is, i is the inclination, an angular measure of the tilt of the orbital plane relative to the reference plane (typically the sky plane), Ω is the longitude of ascending node (typically anticlockwise from North), which orients the orbital plane relative to the reference plane, ω is the argument of periapsis, the angle between the ascending node and the closest point in the orbit (periapsis), and ν is the true anomaly, which defines the position of the secondary at a particular epoch, t_0.

1.1.1 Circumbinary Discs

For angular momentum to be conserved during the star formation process, as some fraction of the star-forming matter moves inwards to form one or more protostars, the residual gas and dust must move outwards to form a circumstellar disc. Viscous stresses within the disc give rise to a process of angular momentum transport, which allows local parcels of gas to lose angular momentum by spiralling in towards the star, while others spiral outwards, leading to a radial spreading of the disc matter and overall redistribution of angular momentum throughout the disc (Shakura and Sunyaev, 1973; Lynden-Bell and Pringle, 1974). The rate at which this movement occurs is dependent on the disc's viscosity – a measure of a fluid material's resistance to changes in motion, also referred to as "internal friction".

This process of disc formation and evolution occurs over several million years, during which, emission from a system will vary. Adams et al. (1987) noted that over time, the maximum observed emission shifts to shorter wavelengths and the optical depth of the system – wavelength dependent measure of how much light is attenuated by a medium (Choudhuri, 2018) – changes. Consequently, Adams et al. (1987) separated these stages of emission into distinct classes, mapping out the time evolution of a young stellar object (YSO). Class I represents a young star with a disc and circumstellar envelope, which produces a large observable infrared excess. Class II describes a classical T Tauri star with a circumstellar accretion disc that is optically thick at wavelengths less than $10\mu m$. By the class III stage, the system has evolved to a weak-lined Tauri star with a circumstellar disc that is optically thin at wavelengths less than $10\mu m$ (André, 2015).

The creation of circumstellar discs is thought to be ubiquitous to the star-forming process, even for multi-star systems (Larson, 2003). Some of these discs can serve as sites for the formation of planetary systems (protoplanetary discs) during their class II phase, whereas other, older discs have passed the age where planet formation is likely to occur (debris discs). The distinction between the two is not clear-cut – in fact, the two are not mutually exclusive as protoplanetary discs are expected to transition into debris discs over time (Wyatt et al., 2015). However, one metric that is often employed to distinguish between them is the optical depth of the disc. A protoplanetary disc can be expected to be optically thick at optical and UV wavelengths, having a higher dust mass than an optically thin debris disc (Wyatt et al., 2015). Debris discs are also typically gas-poor, whereas protoplanetary discs usually have gas-to-dust mass ratios of $\sim$100 (Bohlin et al., 1978). As well as their optical depth, protoplanetary discs have a number of other quantifiable characteristics. The features that are primarily of interest for this project are the disc's mass (comprising dust and gas), size, orbital alignment, viscosity, and dust grain size.

Of the two components that make a disc, gas and dust, the solid dust grains play a greater role in the extinction of light through absorption and scattering. Dust grain size distributions are radius and size-dependent, typically expressed through the power law

$$N(a) \propto a^{-q}, \tag{1.1}$$

where $N(a)$ is the number of grains from a to $a + da$, a is the grain size, and the index q takes on values between 2 and 4 for different models (e.g. Dohnanyi, 1969; Birnstiel et al., 2011). As a result, a disc with a range of grain sizes will have far more smaller grains than larger ones. The sizes of dust grains is significant for two reasons. The first is that a dust particle's grain size sets its Stoker number - a dimensional quantity which is defined as the ratio of the characteristic time of a dust particle to the characteristic time of the fluid flow (Brennen, 2009). The Stokes number, typically denoted St, defines the behaviour of the dust in relation to the gas. It can be safely assumed that, for small dust grains ($St \ll 1$), the dust is well coupled to the gas and the two move together. The second reason is that the wavelength-dependence of extinction is related to the sizes of the dust grains – smaller grains attenuate wavelengths shorter than their size (Andrews, 2020). Consequently, a light source, such as a star, that is occulted by a dust population will be "reddened" by regions of the disc with a higher number density of smaller dust grains. Comparing observations of a disc at different wavelengths can allow us to check for this "reddening" and make inferences about the distribution of dust grain sizes throughout a disc (e.g. Mathis et al., 1977).

It can be expected that the properties of circumbinary discs will largely be determined by interactions with the inner binary, the nature of which are highly dependent on factors such as the disc cavity size, mass, composition and alignment relative to the binary orbital plane. However, a disc will also be heavily influenced by external forces as it evolves over time, such as the effects of photoevaporative winds or truncation through gravitational interactions with nearby stars (Armitage, 2020), especially in binary or higher order systems. Therefore, by observing and studying circumbinary discs, we can gain an understanding of the relationship between the disc and stars in a system and what impact this has on its evolution and dynamics, as well as any planets that may form in the disc.

1.1.2 Star-Disc Interactions

The evolution of a disc's structure is heavily influenced by interactions with nearby stars. Most binaries have separations comparable to typical disc diameters ($\sim 10 - 100$ AU) (Andrews, 2020), so gravitational perturbations in multi-star systems are common. The orbital motion of the binary stars exerts tidal torques on the discs encircling them, leading to angular momentum being transported from the binary to the disc. As a result, the disc's inner edge is truncated, forming a cavity between the disc and binary where disc density is very low, and the inward viscous spreading of the inner edge of the disc is inhibited (Pringle, 1991). The disc inner edge typically settles to about 1.7 times the binary separation (Lubow et al., 2015) but this can vary depending on factors such as the binary eccentricity and disc alignment (Hirsh et al., 2020). Depending on the properties of the disc, the binary's own orbit can also be altered by this loss of angular momentum (Artymowicz et al., 1991; Penzlin et al., 2022).

Just as the disc's inner edge can be altered by interactions with the inner binary, the presence of a massive external body passing close by the disc, whether this is a single encounter or a bound exterior companion, can also lead to the outer edge of the disc being truncated, as disc mass is accreted by the external body (Breslau et al., 2014). In some scenarios, this could instead cause mass to be ejected from the system or even increase accretion onto the central binary. Additionally, an external body can perturb the disc's outer edge, leading to the disc matter being pulled outwards into spiral arms, the disc's inclination being altered and possibly even inducing warps in the disc, distorting the disc's surface (Clarke and Pringle, 1993).

Another factor in the evolution of binary systems is the alignment of the circumbinary disc relative to the orbital plane of the binary. The initial alignment of discs likely depends on the angular momentum of the material which forms the disc, and so chaotic motion caused by turbulence in a molecular cloud can lead to a disc being misaligned immediately after its formation (Bate et al., 2010). Depending on the degree of the initial misalignment, as well as other properties of the system such as the eccentricity and mass ratio of the inner binary, it has been shown that the disc may evolve to become even more misaligned, eventually reaching the stable "polar" configuration, where the disc is aligned ~ 90 degrees to the binary orbital plane (Aly et al., 2015). Alternatively, misalignments could dissipate over time, leading to a coplanar disc (Nixon et al., 2013; Martin and Lubow, 2017; Aly et al., 2018).

1.1.3 Disc Transits

A transit occurs when an object dense enough to occult light passes in front of a star for some period of time, leading to a drop in the flux received from the star (e.g. Armitage, 2020). By measuring the light from a system during a transit, we can produce a light curve – a plot of the observed flux over time. Details of this observable drop in flux, such as its duration and how much light is obscured, can then be used to determine features of the occulting object. Transits are typically associated with the detection of exoplanets, being the method by which the majority of confirmed exoplanets have been discovered to-date (Charbonneau et al., 1999; Dai et al., 2021; Batalha, 2014). However, there have also been documented instances of a star being occulted by the disc of a companion object (Kloppenborg et al., 2010; Gałan et al., 2012; van Werkhoven et al., 2014; Rodriguez et al., 2016). Much like in cases where a star is being occulted by a planet, analysing the light curve of a disc transit can provide crucial information about the structure and composition of a disc, as well as it's motion relative to the occulted object.

For instance, in Rodriguez et al. (2016), the authors report on a red giant being occulted by the circumstellar disc of its companion, a "stripped red giant" subdwarf-B type star. Analysis of key features of the transit light curve, such as changes to the gradient and points of inflections, were used to estimate the radius, velocity and orbital period of the disc. Through employment of a similar method, van Werkhoven et al. (2014), were able to approximate the aspect ratio, diameter and optical depth profile of a circumstellar disc passing in front of the star J1407. Like Gałan et al. (2012) for EE Cephei, van Werkhoven et al. (2014) were also able to infer that the occulting disc most likely has a structure built up of discrete rings of material. In the case of ϵ Aurigae, (Kloppenborg et al., 2010), not only was the disc size estimated using measurements made during the transit, but the size of the disc particles and CO distribution were also approximated, leading to its current interpretation as an optically thick but geometrically thin disc. These examples demonstrate that light curves of disc transits, all of which were conducted at optical wavelengths, encode substantial information about the occulting object and are worth exploring as a means of determining disc properties.

1.2 The HD98800 System

Previous studies of systems that have not been imaged have analysed light curves of the system to constrain disc parameters. For instance, Poon et al. (2021) studied the photometric variability of the KH 15D system with a precessing circumbinary disc, which would obscure light from the inner binary. These observations were used to constrain properties of the disc, such as its precession period and surface density profile. As useful as this may be, it would be ideal to use a system with well-constrained orbital parameters and a disc that can be imaged to study the impact of some of these parameters. This way, existing constraints on the system parameters can be used to produce a set of realistic models, testing different values for unknown parameters, which can then be compared to real observations of the system. HD98800 is one such system, consisting of two binaries, AaAb and BaBb, that orbit a shared centre of mass, and a circumbinary disc around BaBb. Past studies of this system have provided well-constrained estimates for the system's orbital parameters and the disc has been imaged by the Atacama Large Millimeter/submillimeter Array (ALMA) telescope (Boden et al., 2005; Kennedy et al., 2019; Zúñiga-Fernández et al., 2021) and Jansky Very Large Array (JVLA) (Ribas et al., 2018).

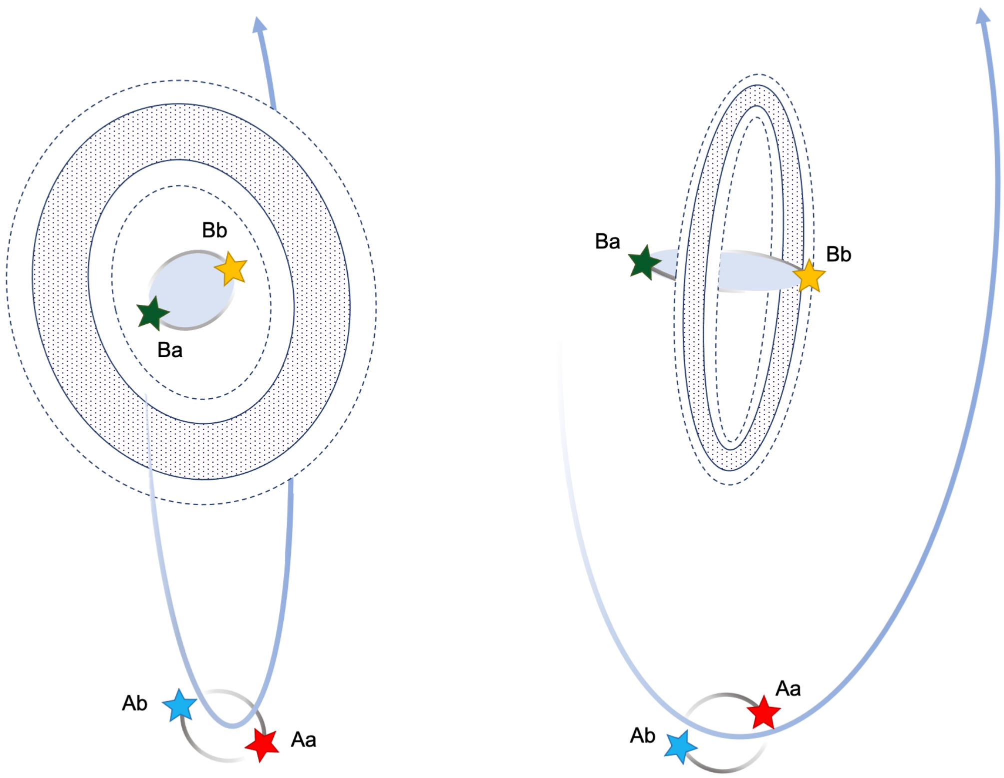

Figure 1.3: Diagrams of sky orbital motion and configuration of the HD98800 system. Left panel: face-on view, right panel: side view. The radial extent of the dust and gas components of the disc are shown by the dotted region and dashed lines, respectively. The motion of AaAb passing behind the disc, as is expected, is indicated by the blue arrow. The light blue shaded region shows the orbital plane of the B binary, inclined almost 90 degrees relative to the circumbinary disc. Not to scale.

1.2.1 System Structure and Parameters

HD98800 is a hierarchical quadruple star system, located 44.9 pc away in the TW Hydrae association (Van Leeuwen, 2007). It comprises two pairs of binary stars, AaAb and BaBb, which exhibit a binary-like motion around each other at a distance of $\sim$ 50 AU. The four stars, Aa, Ab, Ba, and Bb have masses of 0.90, 0.29, 0.77, and 0.62 $M_{\odot}$, respectively. A schematic of the system's configuration can be seen in fig 1.3 and the full set of orbital parameters for the binaries can be found in table 1.1. The binary BaBb has been observed to have a circumbinary disc (HD98800 B) encircling it, which Kennedy et al. (2019), with confirmation from Franchini et al. (2019) and Zúñiga-Fernández et al. (2021), have inferred to be misaligned by around 92 degrees relative to the orbital plane of BaBb, making it the first known protoplanetary, polar aligned disc. N-body simulations were used by Kennedy et al. (2019) to demonstrate that a gas-free disc could not survive in such a system, irrespective of the disc orientation, leading to the interpretation of HD98800 B as a gas-dominated disc with a dust component extending from 2.5 to 4.6 AU and a gas component from 1.6 to 6.4 AU, based on ALMA observations. It is assumed that the gas component is mostly hydrogen, although the bulk gas distribution has been traced using carbon monoxide. Kennedy et al. (2019) also provide lower bound estimates for the dust and gas mass of 0.33 $M_{\oplus}$ and 0.28 $M_{\oplus}$, respectively. However, these estimates are based on ALMA observations of emission at millimetre wavelengths, at which the disc may be optically thick for both dust and CO, hindering our ability to see emission from all of the material, so the actual mass of the disc, or either of its individual components, may be higher.

	a (AU)	e	i (deg)	Ω (deg)	ω (deg)	nu (deg)	Period (years)
AaAb	0.86	0.4808	-135.6	170.2	-111.3	194.34	0.724
BaBb	1.01	0.805	-66.3	342.7	-75.5	189.16	0.862
AB	51	0.460	-88.1	184.5	-115	250.7	230

Table 1.1: Orbital parameters for the binaries AaAb, BaBb, and AB, adjusted from Zúñiga-Fernández et al. (2021) to the reference time of $t_0 = 2023$.

1.2.2 Anticipated Transit

According to Zúñiga-Fernández et al. (2021); Kennedy et al. (2019), in 2026 the binary AaAb will pass behind the disc around BaBb, resulting in an observable drop in stellar flux received from Aa and Ab. Much like in the examples provided above, we anticipate measurements made of this transit could be used to constrain a number of disc properties directly through analysis of the system's light curve. However, by providing a preliminary analysis of this transit based on simulation data, we can also offer some guidance on what to expect and what inferences can be made by comparing the simulation data to the real data.

The transit will last approximately a decade, with three distinct sections: the first as the stars Aa and Ab pass upwards behind the lower half of the disc, then another as these stars pass behind the disc cavity, allowing us to study what the density profile of disc material looks like inside the cavity of the B binary, and a final section as the stars pass behind the upper half of the disc. Assuming the disc is axisymmetric, we expect the first and last sections to somewhat resemble a mirror-image of one another, with minor differences arising due to Aa and Ab passing behind each section of the disc at different phases in their orbits i.e. their true anomalies would differ.

As the stars pass behind different sections of the disc, the fractional drop in flux can be used to calculate the optical depth at different disc radii, which in turn can provide a clearer picture of the distribution of dust throughout the disc. The disc edges can be constrained by considering the width of the dips associated with the first and last portion of the transit and by defining some optical depth beyond which the disc is considered to begin. Any non-axisymmetric features in the disc may also be identifiable by some smaller-scale regions of higher or lower disc density in the light curve of the transit. By creating light curves based on simulations of such a system, the effects of a number of other properties can be studied and provide further features to anticipate during the real transit. The effects of properties such as the disc's viscosity and gas-to-dust mass ratio can also be studied by identifying how features in the light curve of the transit may differ between simulations where only a single property of the disc is being varied. Additionally, these preliminary light curves can be used to make informed decisions about future observations of the system and transit, such as the ideal cadence of observations required to see any scientifically interesting features. In line with past observations of occulting discs (see section 1.1.3), these synthetic observations will be generated at an optical wavelength ($0.8\mu m$), as the stars will be harder to detect at longer wavelengths.

1.3 Project Objectives

Based on what is already known of the system prior to this transit, we can run N-body and hydrodynamical simulations of the HD98800 system to consider what may be observed during this transit event. This would involve simulating the system for the duration of the transit, making some reasonable assumptions about the disc properties, and using the simulated data to generate light curves that capture the anticipated drop in flux corresponding to the stars passing behind the disc. By creating synthetic observations of the transit for different disc parameters, we can establish how features observed in the light curve relate to characteristics of the disc. Currently, the disc extent and alignment, and orbital parameters of the stars are well-constrained (Tokovinin, 1999; Boden et al., 2005; Zúñiga-Fernández et al., 2021), but many properties of the disc, such as its mass, viscosity, and gas-to-dust ratio are not. Hence, for the disc parameters which are not well-constrained, a grid of simulations can be created and run to study the differences that result from varying these parameters.

Overall, the aims and motivation behind this project are as follows:

(i) To generate a grid of computational models of the HD98800 system, defined by a parameter space that encompasses the range of values we would reasonably expect, given what is already known about the system. For instance, we expect the disc to be optically thick (Kennedy et al., 2019) and know what the thermal emission for the disc should look like (Ribas et al., 2018), allowing us to limit the dust masses we need to test.

(ii) To compare models that differ by a single parameter value and consider what observable effect this parameter has on the light curve of the transit. This information will be especially useful to those analysing and interpreting data from the real transit in a few years time.

(iii) To suggest some possibilities of what the real transit light curve may look like, based on what is already known of the system. This can also provide context for future observations – what light curve features should be anticipated when observing the transit in the years to come and what cadence is required to ensure those features are visible?

(iv) As well as providing a some preliminary guidance for the transit, hydrodynamical models can be compared to existing ALMA observations to constrain some disc properties, such as the disc's dust mass or radial extent.

(v) By conducting radiative transfer calculations at different wavelengths and comparing the resultant data, the wavelength dependence of observations can be considered. This can also inform future observations of the system – at what wavelength(s) should the system be imaged?

The goal of this research is to help inform future study of the HD98800 system, as well as furthering our current understanding of circumbinary disc properties and binary systems in general. While all of the objectives outlined here are discussed in this thesis, due to time constraints, only (i) to (iii) were completed.

Chapter 2

Computational Methods and Theory

Given that the primary goal of this research is to inform observations of the future transit of HD98800 B in front of AaAb, as well as subsequent study of the system, it is reasonable to pose the following questions: (i) which system properties affect the light curve of the transit and (ii) what effect do each of them have on the observations? To answer these questions, simulated versions of the system and transit can be made with varying disc properties and these models used to create light curves that indicate what the transit may look like to an observer i.e. synthetic observations (e.g. Haworth et al., 2018). The resulting light curves for different disc models can then be compared to answer the questions above. To produce these simulations and synthetic observations, a host of existing software was used. This chapter will cover the computational techniques utilised for this project, how they were used, and why. I will begin by providing an overview of the method used to generate synthetic observations of the HD98800 system, followed by descriptions of each of the software used and how. Once the complete pipeline for production of results is understood, I will outline how the input parameters were chosen and fed into this pipeline, leading to the results seen in chapter 3.

2.1 Generalised Approach to Creation of Synthetic Observations

Broadly, the method used for the creation of light curves involved the following steps:

(i) A simulation of the HD98800 system was generated that was capable of simulating the motion of all four stars and the circumbinary disc. The stellar motion could be modelled relatively simply using N-body calculations, since it is only dependent on the gravitational interactions between the stars, with the disc mass having a negligible effect. In order to model the disc, two different methods were employed – in one case a static disc was superimposed on top of a simple four-star N-body simulation and in another, the disc was modelled using hydrodynamical software, which was able to simulate the fluid motion of the disc and thus, account for disc properties such as viscosity and gas pressure. In each case, the orbital elements given in Zúñiga-Fernández et al. (2021) were used, after adjusting the stellar true anomalies given so the entire system was starting at the same epoch.

(ii) The system was shifted into the reference frame of the centre-of-mass of BaBb so that the disc, which is centred on the centre-of-mass of BaBb is fixed at the origin. The start time of the simulation was set to be a few years prior to when Aa and Ab would approximately begin to pass behind the disc, bearing in mind that exactly when this occurred was dependent on the disc's optical depth profile and so varied across different models.

(iii) Taking a sky plane projection of the simulated disc at each timestep, the optical depth of the disc was calculated along the line-of-sight at each location of the grid. This produced a set of optical depth maps of the disc, each one corresponding to a timestep in the simulation.

(iv) At each timestep, the Cartesian coordinates of the stars Aa and Ab were read from the corresponding simulation data. The disc optical depth $\tau(\lambda)$ that corresponds to the location of each of the stars was then obtained by projecting the stellar coordinates onto the optical depth map for the corresponding timestep. Then, the flux received from each star at that timestep could be calculated as

$$F(\lambda) = F_0(\lambda)\exp(-\tau(\lambda)) \tag{2.1}$$

where F_0 is the incident flux from the star. The ratio of the fluxes of Aa to Ab was obtained by comparing stellar atmosphere models and found to be 3.9 at our chosen wavelength of 0.8 μm. The total flux of AaAb at a given wavelength was obtained by interpolating the values found in table 2 of Ribas et al. (2018). From these values, the individual fluxes of Aa and Ab could be calculated.

(v) The total flux from Aa and Ab was then added to the total flux from BaBb (assumed to be constant over the duration of the simulation) and plotted over time to produce a light curve of the entire system during the transit.

In the following section, I will detail the first application of this method, which used an N-body simulation code.

2.2 N-Body Simulations

`REBOUND` (Rein and Liu, 2012; Rein and Spiegel, 2015) is an N-body code that can be used to simulate the motion of point-mass particles under the influence of gravity. It is a fast and computationally efficient method for calculating the motion of astrophysical bodies that can be modelled as gravitationally-interacting particles, such as stars or planets. It is less effective for modelling the motion of a fluid medium like an accretion disc as it cannot simulate fluid properties such as viscosity and pressure. Nonetheless, `REBOUND` can be used to model the motion of the four stars of HD98800 and, by superimposing a static disc with distinct edges and a chosen optical depth profile onto the results, can be used to create a simplified light curve of the system.

2.2.1 Setup of `REBOUND` Simulation

`REBOUND` was used to model a quadruple star system with no disc, using the parameters provided in Zúñiga-Fernández et al. (2021). These are defined with reference to a "primary" body for each of the three binaries (two binary star systems, AaAb and BaBb, and the wide binary AB). In order to create a hierarchical quadruple system using the given parameters, each step in the hierarchy had to be built sequentially. Initially, the wide binary was constructed, consisting of two "stars" representing the centres of mass of A and B. Then, two smaller binary systems were constructed, representing AaAb and BaBb. The BaBb system was then substituted for B and AaAb for A in the wide binary simulation. The resulting simulation could then be integrated forwards in time, as the stars Aa and Ab passed behind the space where a disc would be. The results shown in fig C.1 of Zúñiga-Fernández et al. (2021) were reproduced (see fig 2.1a), confirming that the binary orbital parameters do indeed predict a transit beginning in around 2026. The values obtained from this model for the locations of the stars could then be used to create a light curve of the transit, under several simplifying assumptions about the disc.

Aside from the light curve, this model was also used to (a) compare the stellar trajectories to those produced in the hydrodynamical simulations and ensure that the orbital parameters being used in both simulations were correct, accounting for any differences in how the parameters were defined by each piece of software, and (b) check the timing of the transit and easily calculate orbital parameters for different times in the simulation, since `REBOUND` can be used to integrate a simulation to a chosen timestep, then output all orbital parameters at that time.

2.2.2 Generation of Simulated Light Curves

Based on the stellar trajectories calculated using the `REBOUND` model, a light curve of the transit was created, assuming the existence of a static disc around BaBb with a simple optical depth profile $\tau = 0.5r_0/r$, where r_0 is the semi-major axis of the disc's gas inner edge at 1.6 AU. The disc was defined only within the region where 1.6 AU $< r <$ 6.4 AU i.e. the radial extent of the CO component of the disc measured by Kennedy et al. (2019), with a sharp cut-off at the disc edges. Here and later, we assume that the dust causing the optical transit is small and therefore well coupled to the gas.

Once a disc with a defined optical depth profile had been "added" to the simulation, a simplified light curve of the transit could be made by following the steps outlined in section 2.1. The simulation was integrated forwards in time and at each timestep, the positions of stars Aa and Ab and the optical depth profile defined above were used to calculate the value of τ at each star's location. Then, the corresponding drop in flux for each time could be calculated using eq 2.1 and plotted over time. However, the major drawback of this method was that factors such as disc mass, viscosity and the distribution of gas and dust matter were not accounted for here, as `REBOUND` does not have the functionality to simulate some of these properties. To model these properties of a disc, hydrodynamical simulations, capable of simulating the dynamics and evolution of a viscous, pressure-supported disc, were needed. The results of these N-body and all hydrodynamical simulations will be discussed in chapter 3.

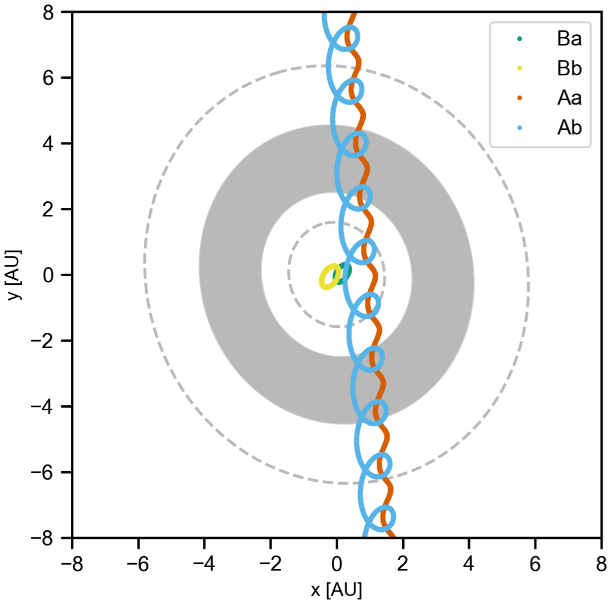

(a) The radial extent of each component of the disc, according to Kennedy et al. (2019). The solid grey region indicates the dust component of the disc (2.5 to 4.6 AU) and the dashed lines show the radial extent of the gas component (1.6 to 6.4 AU).

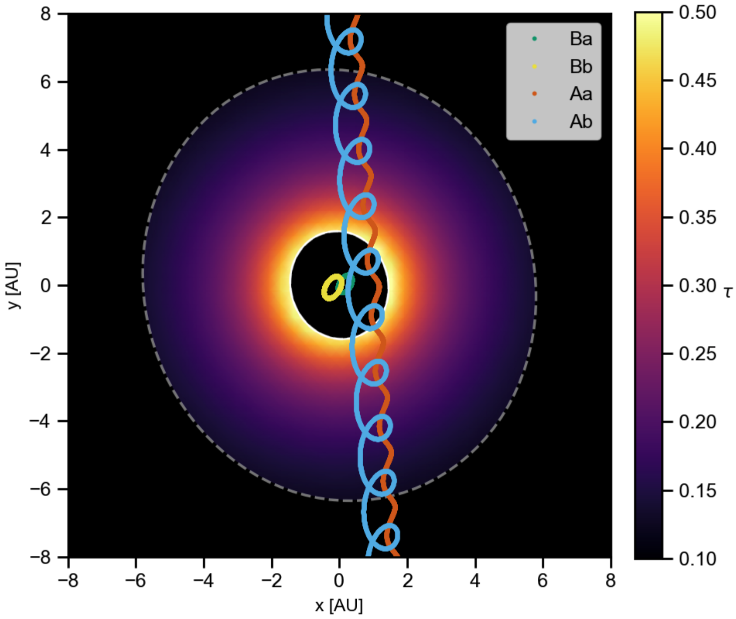

(b) The assumed radial optical depth profile for the `REBOUND` light curves. The dashed lines indicate the cut-off where the disc edges are defined (1.6 and 6.4 AU for the inner and outer edge, respectively).

Figure 2.1: The orbital motion of the 4 stars relative to the centre of mass of BaBb, calculated using `REBOUND`, along with the gas component of the disc superimposed onto the grid.

2.3 Hydrodynamical Simulations

Smoothed Particle Hydrodynamics (SPH) is a computational method used to simulate a fluid medium, such as the gas and dust components of a circumstellar disc, by numerically solving equations of fluid motion (Lucy, 1977; Gingold and Monaghan, 1977). The basic principle of SPH involves the discretisation of a fluid onto a set of particles that are each characterised by properties such as mass, velocity and energy. The movement of these particles is calculated over time as an SPH simulation progresses, accounting for interactions between neighbouring particles, and the properties of particles at a given location is used to determine the bulk properties of the fluid at that location, such as fluid viscosity or density. SPH has a number of features that makes it useful for modelling accretion discs, one of which is its computational efficiency through the use of density-scaled resolution, allowing for finer detail to be measured in regions where the disc density is greater to provide more accurate results. One particularly advantageous feature of SPH is that, due to the lack of grid, there is no possibility for grid geometry to influence the motion of disc material, as can sometimes be the case for grid-based hydrodynamical simulations. This is an important consideration for modelling the disc of HD98800, as its eccentricity, tilt, and slight precession mean that modelling it with a grid-based approach may present difficulties.

`Phantom` is an open-source SPH code written in Fortran 90 that has been designed with a focus on efficient modelling of accretion discs, as well as other astrophysical objects (Price et al., 2018). Crucially, `Phantom` allows for the creation of a fully configurable disc, modelled using the desired number of SPH particles, with a chosen dust-to-gas ratio, mass, and viscosity, allowing for the creation of a set of of models where each of these parameters is varied individually to test their effect on the resultant light curves in isolation of any other changes. Consequently, `Phantom` was used to create a grid of hydrodynamical models of the stars and disc of HD98800, which were used to test the effects different disc properties had on synthetic observations of the system.

2.3.1 Model Setup

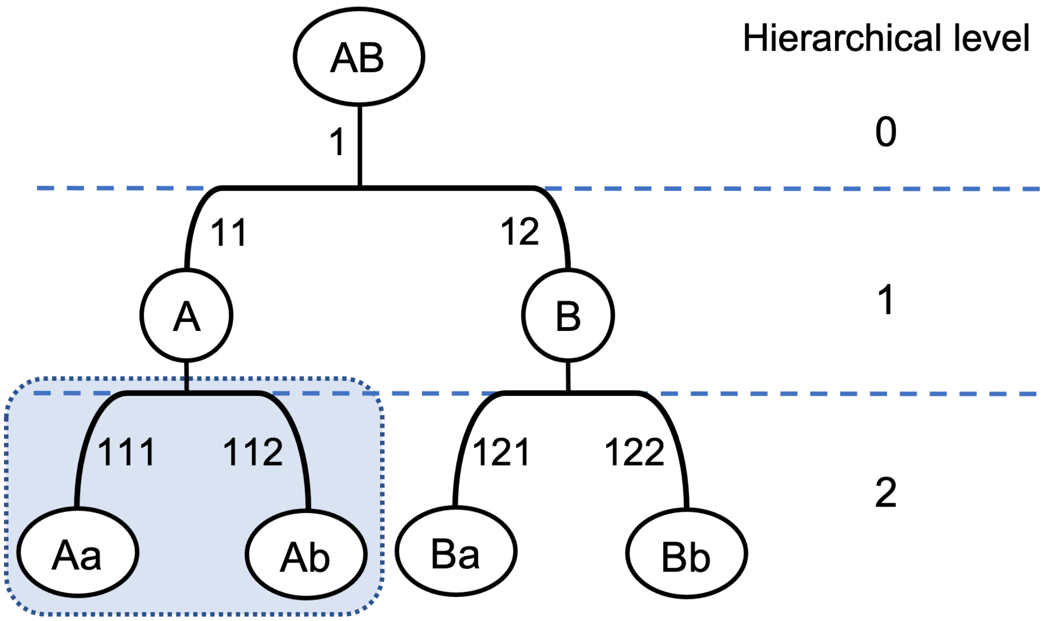

Figure 2.2: Mobile diagram of the hierarchical levels of HD98800. Each hierarchical level is labelled using subsytem notation from Tokovonin's Multiple Star Catalogue (Tokovinin, 2018). The area contained within the shaded blue region indicates the changes made to `Phantom` i.e. the splitting of the first hierarchical level primary star into a binary system.

`Phantom` allows for the creation of hierarchical multi-star systems with discs, defining "sink" particles to represent stars (Bate et al., 1995). A system with a single star is created with the star fixed at the origin. For any higher order system, each hierarchical level is created with a secondary body defined with respect to a primary body. A number of different "setup" types are enabled in `Phantom`. For the purposes of this project, the `disc` setup was required to create a hierarchical quadruple system with a circumbinary disc. However, at the time this project was initially undertaken, the `disc` setup module for `Phantom` could only construct systems with a maximum of three sink particles. As a result, the `Phantom` source code needed to be modified to enable the creation of a hierarchical quadruple system.

To achieve this, the existing code for the construction of a hierarchical triple system was extended to allow for the creation of a hierarchical quadruple. `Phantom` creates a hierarchical triple by initially creating a "wide" binary system, with a primary sink located at the origin and a secondary sink with its orbital elements defined with respect to the primary. Then, using the same subroutine that was used to construct this binary, a second “tight” binary is constructed, centred on the location of and replacing the secondary star. This leads to the creation of a hierarchical triple, consisting of a primary star on the first hierarchical level as well as a secondary on the first hierarchical level which splits off into a second hierarchical level that consists of another binary star system. To create a hierarchical quadruple, the same process used to create the second hierarchical level from the first hierarchical level secondary could be repeated for the first hierarchical level primary, creating two “tight” binaries that orbit each other in a “wide” binary (see fig 2.2). In the end, the hierarchical quadruple could be defined entirely in terms of 3 binary systems – one “wide” binary describing the motion of A relative to B, followed by the two “tight” binaries AaAb and BaBb, defined with respect to Aa and Ba respectively. This was similar to how the quadruple star system was created in `REBOUND`, as described in section 2.2.1.

The orbital parameters of the stars and any parameters used to define the circumbinary disc could then be input to the `.setup` file and read by `Phantom` to set up the simulation. For all simulations run as part of this project, a disc surface density profile $\Sigma(r) \propto r^{-p}$ was used, with a p value of 1, and a radial temperature profile $T(r) \propto r^{-q}$, with a q value of 0.25. Once the motion of the stars had been correctly defined, the centre-of-mass of BaBb was calculated and set as the location for the centre of the circumbinary disc.

2.3.2 Disc Transients

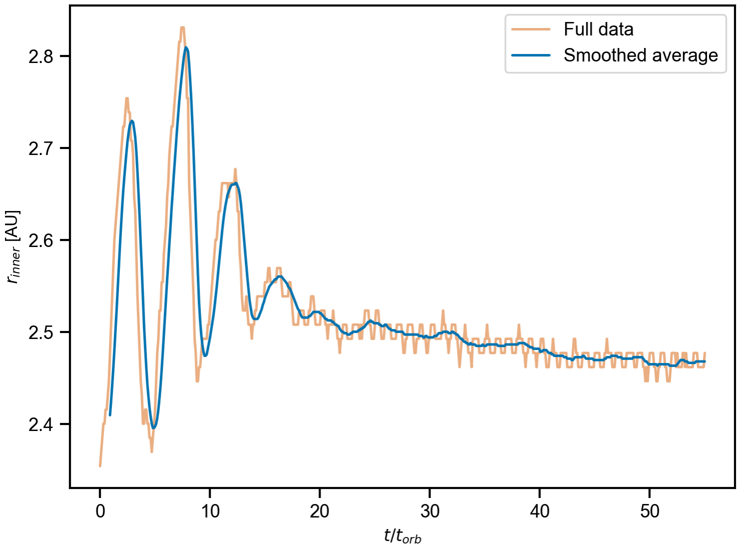

Figure 2.3: Size of the disc cavity in a gas-only `Phantom` simulation of HD98800 over time.

At the start of a simulation, `Phantom` initialises SPH particles on Keplerian orbits around the centre-of-mass of BaBb, treating the centre-of-mass as a point mass. However, once the simulation begins, the binary orbits exert gravitational effects on the SPH particles, altering their orbits. As a result, the simulations needed to be run for a period of time prior to the transit to allow the transients to be "washed away". Past studies have looked at the time needed for a disc to settle into a steady-state in the presence of an inner binary star system (Franchini et al., 2019; Ragusa et al., 2020; Hirsh et al., 2020), determined by the size of the disc cavity, defined as the radius at which the disc surface density was greater than some fraction of the maximum surface density. In general, it was found that a disc with an inner binary mass ratio similar to that of BaBb reached this state within about 100 orbits of the inner binary. Although these studies do not consider a second, outer binary potentially perturbing the disc's outer edge, and most assume the disc to be in a coplanar configuration, these results provided an estimate for how long the models of HD98800 should be allowed to run before the transit observations could begin to ensure that any features observed in the light curve are not due to any transients.

To test this with my own models, a simulation was run for an extended period of time without the outer binary, to determine how long it took the inner edge of the disc to settle under the perturbing effects of the inner binary. For this work, the fraction of the maximum surface density that was used to define the inner edge of the disc was 25%. The results of this, shown in fig 2.3, indicated that a duration of 40 inner binary orbits ($\sim$ 34.5 yrs) would be sufficient for running the models prior to the transit, as it was found that the disc inner edge did not vary significantly past this point, settling to a value of $\sim$ 2.5 AU.

Past studies (Artymowicz and Lubow, 1994; Hirsh et al., 2020; Ragusa et al., 2020) have considered the relationship between disc cavity size and the binary separation. In general, it has been shown that the disc cavity is typically found to be approximately 1.7 times the binary separation (Facchini et al., 2018). For BaBb, which has a binary semi-major axis of 1.01 AU, this would correspond to a disc cavity size of $\sim$ 1.7 AU. However, the binary mass ratio, eccentricity, and the disc's inclination are all expected to have some effect on the steady size of the disc cavity. BaBb has a mass ratio of $0.62/0.77 = 0.805$ and eccentricity of 0.805, as well as a polar-aligned disc. It is expected that the high eccentricity and high mass ratio of the binary would increase the cavity size (Hirsh et al., 2020), although the high inclination of the disc may offset this effect (Lubow et al., 2015). It is also worth noting that the accretion radius for the inner binary stars was set to 0.1 AU in all models, since a lower accretion radius may have been computationally prohibitive. This may have increased the cavity size by a small factor as well.

A simulation that included the outer binary was also run for an extended period of time, and found that the presence of an outer binary passing closing enough to the outer edge of the disc can cause perturbations once per passage (see section 3.2.1), preventing the outer edge from settling over long-scale periods, although any short-term transient behaviour due to the initialisation of the SPH particles did disappear within a few inner binary orbits, as expected. Once this steadying period and all variable parameters had been decided, the grid of models was created and run for the total duration of time needed to capture the passage of AaAb behind a steady disc. It was found that 15 inner binary orbits ($\sim$ 13 yrs) was sufficient for this in most cases. The one exception to this was a longer simulation that was run with a slightly larger disc, which had a slightly prolonged transit. To ensure that time resolution was not a limiting factor in our ability to quantify light curve features, the time between consecutive outputs, Δt, was set to be 1/100th of an inner binary orbit ($\sim$ 3.1 days).

2.4 Radiative Transfer Modelling

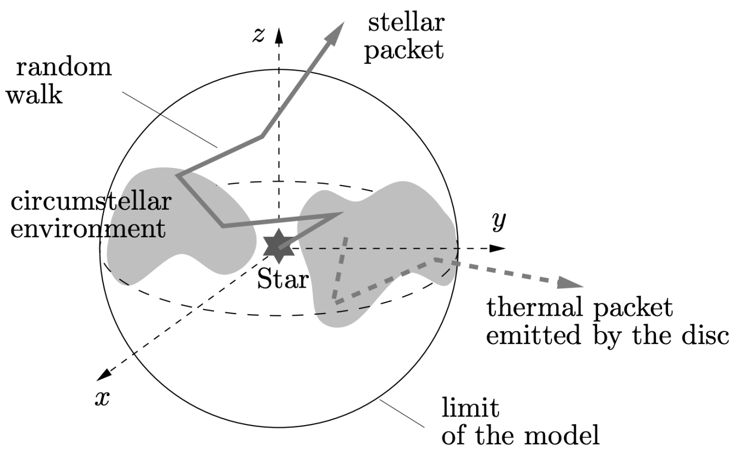

Figure 2.4: Schematic showing how the motion of photon packets is tracked through `MCFOST` to create synthetic observations (Pinte, 2015).

Radiative transfer modelling refers to the process of modelling light interactions such as scattering and absorption in a radiative medium. `MCFOST` is a three-dimensional radiative transfer code that uses the Monte Carlo method to calculate optical quantities for a simulated system. It works by tracking the motion of individual photon packets as they propagate through the simulated environment, taking into account scattering, absorption, and re-emission events, until they exit the computational grid and are "observed" (Pinte et al., 2006, 2009).

`Phantom` output data can be projected onto an `MCFOST`-generated grid and used to calculate optical properties of a system at a chosen wavelength, allowing for the creation of images, spectral energy distributions (SEDs) and light curves of the simulated system. Using `MCFOST` with `Phantom` is especially useful since `MCFOST` can be used to assume the presence of of a chosen proportion of dust for a gas-only `Phantom` simulation. This means that `Phantom` simulations for a system where we can reasonably assume the dust and gas to be strongly coupled can be run as gas-only simulations, reducing the total runtime, and dust added at the radiative transfer step using `MCFOST`, assuming the gas and dust particles have the same density distribution. To ensure the validity of this assumption, the dust grain size distribution was configured accordingly. For the gas-only simulations, dust grains ranging from a size of $0.03 - 1000\mu m$ were used, with a distribution described by eq. 1.1 with $q = 3.5$. These sizes of dust grains should be low enough that the dust and gas are strongly coupled in the simulations (the Stokes number is $\sim 10^{-5}$-$10^{-4} \ll 1$ for the smallest dust grains). To ensure sufficient resolution, the number of photon packets for temperature calculations was set to 1.28×10^8.

`MCFOST` was then used to generate three-dimensional optical depth maps for each timestep in the simulations, using the `Phantom` outputs to do so. To produce these maps, the visualisation tool `SPLASH` (Price, 2007) was used to generate a density grid in cylindrical coordinates for each timestep in the simulation. An `MCFOST` spatial grid was created and the `SPLASH` grid used to interpolate density values onto the `MCFOST` grid cells. `MCFOST` was then run on this density grid to calculate optical depth values at the chosen wavelength in r and ϕ, summed in the z direction. The positions of the stars at each timestep were obtained from the `Phantom` output files and multiplied by -1 to account for the fact that `MCFOST` grids have reversed axes. At each timestep, the optical depth at the locations of Aa and Ab could then be interpolated from the corresponding optical depth map. The flux from each star at each timestep could then be calculated using eq 2.1 and plotted over time to produce a light curve.

Through the use of `MCFOST` for handling radiative transfer calculations, hydrodynamical simulations produced using `Phantom` could be used to generate optical light curves of the HD98800 system and transit for a host of different system parameters (`Phantom`) and radiative parameters (`MCFOST`).

2.4.1 Generation of Simulated Light Curves

For each of the models in the grid, the following steps were taken to produce a synthetic light curve, based on the computational techniques outlined in this chapter:

(i) `Phantom` simulations were run using my own updated version of the source code. These simulations used the orbital parameters found in table 1.1, which were adapted from Zúñiga-Fernández et al. (2021) so that the simulation began about 40 inner binary orbits prior to the approximate start of the transit, to allow any transients to dissipate. The initial disc radius for all simulations was set to be equal to the dust radius given by (Kennedy et al., 2019) (2.5 to 4.6 AU), though, as show in fig 2.3, the disc spreads slightly to reach a near steady-state. The one exception to this was the fiducial model, which was set to have a higher disc radius (6 AU) to consider what unique features, if any,

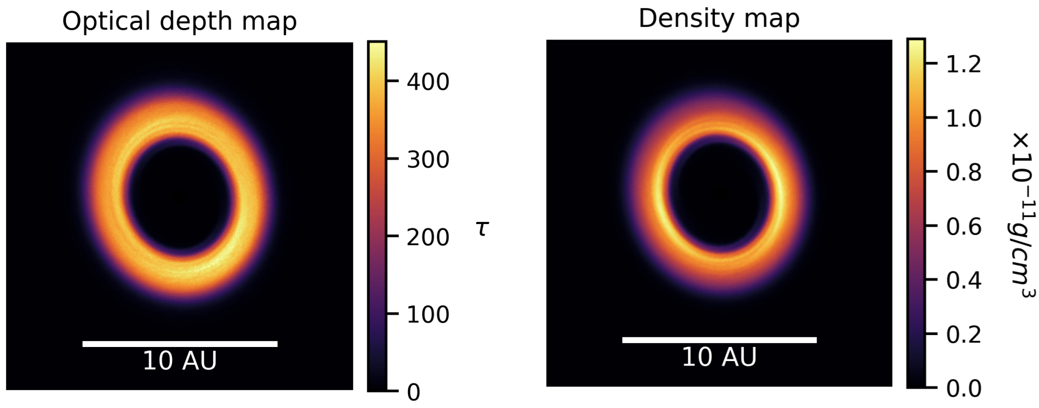

Figure 2.5: Outputs showing the sky plane projection of the fiducial simulation (see table 2.1), generated using MCFOST and used to produce light curves. Left: optical depth map. Right: density map.

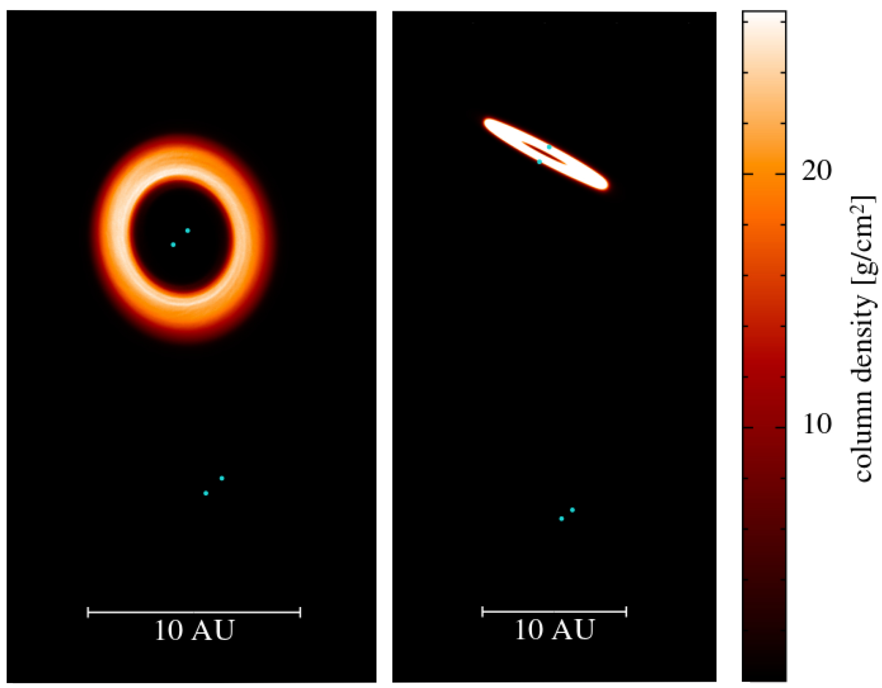

Figure 2.6: Images generated using SPLASH showing the sky plane projection of the column density of a gas-only disc. Cyan markers indicate the four stars.

would be visible in the light curve and whether any longer-term effects could be observed for a slightly larger disc. The disc was modelled using 10^6 SPH particles, to ensure resolution was not a limiting factor in the quality of the results.

(ii) `Phantom`'s built-in "moddump" functionality was used to modify the dump files (`Phantom` output files) such that the centre-of-mass of BaBb and its circumbinary disc are fixed at the origin, with the locations of stars Aa and Ab being defined in the reference frame of the centre-of-mass of BaBb.

(iii) `SPLASH` was used to create three-dimensional density grids for each `Phantom` output. These consisted of ASCII files containing the density distribution of the SPH particles in the simulation on a Cartesian grid.

(iv) A cylindrical `MCFOST` grid of a chosen grid size and resolution was created (300 cells in the r direction, 200 cells in the z direction, 250 cells in the ϕ direction). The data from the `SPLASH`-generated density grids was then converted to cylindrical coordinates, projected and interpolated onto the `MCFOST` grid.

(v) `MCFOST` was then used to calculate the optical depth of the disc, summed in the z direction, in each cell of the density maps generated in the previous step. These values were saved in a 300×300 two-dimensional grid, spanning 40 AU in the x and y directions. This created a series of optical depth maps where each optical depth map corresponded to a timestep in the simulation.

(vi) Each optical depth map was used to calculate the optical depth of the disc at the location of stars Aa and Ab at each timestep. This was achieved by reading the star's locations at a given timestep from the `Phantom` `discSink*.ev` output files and finding the value of the disc's optical depth in the corresponding grid cell of the optical depth map for that timestep.

(vii) The data for all timesteps was collated and used to calculate the flux drop from each of the stars using eq 2.1. The incident flux values at the chosen wavelengths were interpolated from values found in Ribas et al. (2018). Then, the time-varying flux from Aa and Ab could be calculated and added to the flux from BaBb (assumed to be fixed, value also taken from Ribas et al. (2018)). This was then plotted over time to produce a light curve of the transit.

2.5 Developing the Parameter Space

The final set of parameters input to `Phantom` simulations and `MCFOST` calculations are summarised in the tables below. This section outlines how these parameters were chosen. Throughout chapter 3, the models will be referred to by their combination of `Phantom` and `MCFOST` parameters e.g. model 1A refers to `Phantom` model 1, with the parameters described by `MCFOST` model A.

`Phantom` Model	Disc Mass ($M_{\oplus}$)	Gas-Dust Ratio	Dust Grain Size (cm)	α
1	3.3	-	-	0.005
2	33	-	-	0.005
3	330	-	-	0.005
4	33	-	-	0.01
5	33	-	-	0.05
6	33	100	0.13 (St $\simeq$ 0.03)	0.005
7	33	100	1.00 (St $\simeq$ 0.25)	0.005

Table 2.1: Grid of parameters for the `Phantom` simulations run. All simulations except for 7 and 8 were run as gas-only simulations, with dust added later, at the radiative transfer step. Stokes numbers have been given for the two-fluid simulations.

`MCFOST` Model	Dust Mass ($M_{\oplus}$)	Wavelength (μm)
A	0.033	0.8
B	0.33	0.8
C	3.3	0.8

Table 2.2: Parameter space for `MCFOST` radiative transfer calculations. Each of the `Phantom` simulations in table 2.1 was run with one or more of these sets of `MCFOST` parameters.

2.5.1 Constraining Dust and Gas Mass

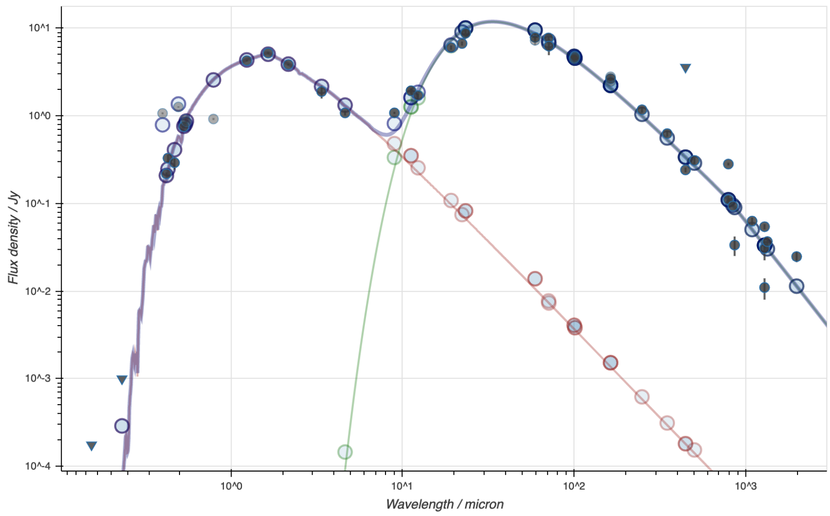

Figure 2.7: SED of the HD98800 system based on various past observations. Dots show observations and lines model the components – the stars and a dust disc. Open circles show the values expected for the model components at each observed wavelength. Noisy behaviour seen at mm wavelengths may be due to these data points corresponding to older surveys, which may have underestimated the errors on their measurements. Credit: Kennedy, Grant M (2020).

Spectral energy distributions (SEDs) describe the disc emission at different wavelengths, allowing us to characterise the source of the radiation (e.g. Armitage, 2020). We anticipate disc emission to be dominated by thermal emission from dust particles so by studying SEDs of HD98800 B, we can constrain the total dust mass of the disc. By comparing simulated SEDs of the HD98800 system for different dust masses and a fixed dust grain size distribution to the observed SED of the system, an order of magnitude estimate for the dust mass can be obtained.

To do this, `MCFOST`'s built-in SED generation function was used. A single `Phantom` output file was chosen to generate the SEDs, which was associated with a timestep prior to the start of the transit and after the disc had reached its steady-state. A series of SEDs were then created, each with different input values for the dust mass. The values chosen for this were all factors of 10 apart, starting with the estimate provided in Kennedy et al. (2019) of $0.33M_{\oplus}$ for the dust mass. The effect of changing the gas mass was assumed to be negligible. The data points from the observed SED (fig 2.7) were then plotted on top of the SEDs generated using `MCFOST` to compare the emission from the simulations at different dust masses to that of the real system.

The results of this can be seen in fig 2.8, where the SEDs for the three dust masses that approximately lie closest to the observed the SED have been plotted with the data points from fig 2.7. Although none of these perfectly match the observed emission at all wavelengths, this could be due to a number of factors other than the dust mass. For instance, there are uncertainties associated with the estimated radial extent of the disc, so the real size of the disc may differ from the `Phantom` simulations. The creation of the SEDs also necessitated making certain assumptions when carrying out radiative transfer calculations in `MCFOST`, such as the distribution of dust grain sizes and the temperature structure of the disc, which may differ from that of the real disc. Since the wavelength of emission from the dust component is heavily dependent on the sizes of the dust grains, this could also lead to discrepancies when compared to the observed SED. In general, constraining disc properties using SEDs is a degenerate problem – a number of different physical processes can lead to the same changes in an SED.

Based on this comparison, three dust masses that seemed to be of an appropriate order of magnitude were chosen as the three different dust masses to use in the grid of models. These were $0.033M_\oplus, 0.33M_\oplus$, and $3.3M_\oplus$. The gas masses to be input to the `Phantom` simulations were chosen based on these three values by taking the canonical interstellar medium gas-to-dust mass ratio of 100 (Bohlin et al., 1978) to be reasonably applicable to circumstellar discs, leading to the three tested gas masses of $3.3M_\oplus$, $33M_\oplus$ and $330M_\oplus$. The median values for the dust and gas masses were used for the fiducial simulation – $0.33M_\oplus$ and $33M_\oplus$ for the dust mass and gas mass, respectively.

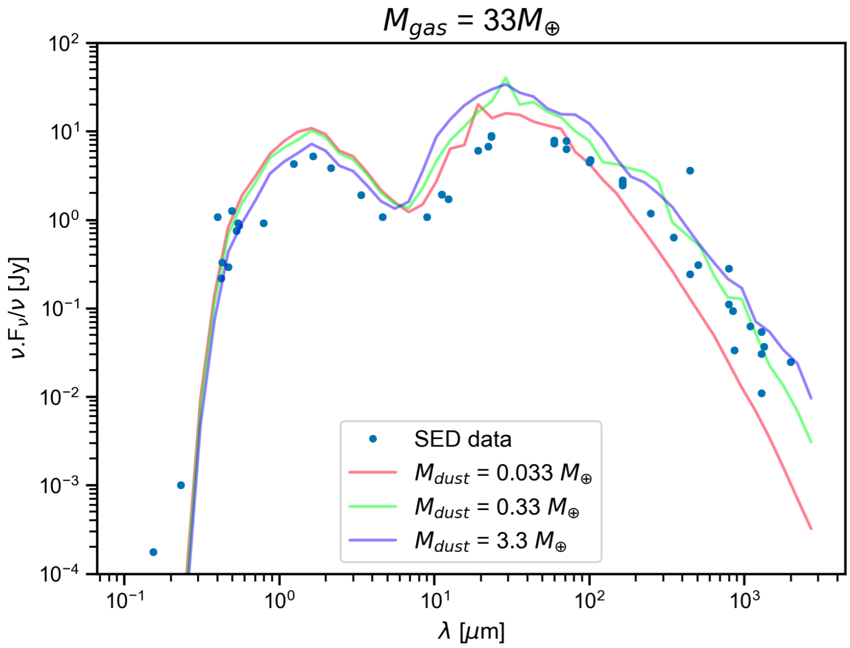

Figure 2.8: SEDs produced for disc with a gas mass of $33M_\oplus$, using different dust masses, plotted on top of the observed SED data points from fig 2.7.

2.5.2 Other Parameters

Having chosen a reasonable range of dust and gas masses to test, the remaining disc parameters needed to be selected. The range of values for the viscosity parameter α was chosen based on a combination of factors. The first of these is the physical constraint that $\alpha \leq H/R$, where H/R is the disc's aspect ratio (ratio of scale height to disc radius). The second consideration involved looking at past viscosity measurements of protoplanetary discs, based on observations and models, to discern a reasonable range of values. For instance, Rafikov (2017) found a range of $\sim 10^{-4} - 10^{-2}$, based on ALMA observations. Papaloizou and Nelson (2003) and Steinacker and Papaloizou (2002) both produced disc models to study the magneto-hydrodynamic evolution of a disc until it reached a turbulent state, then measured the resultant value of α to be, on average, 0.005 and 0.004 ± 0.002, respectively. As a result, the three α values chosen were 0.005, 0.01, and 0.05, the largest being equal to the aspect ratio H/R. However, given that there are no current constraints on the viscosity of the disc of HD98800, the value of α for the fiducial model was chosen to be 0.005.

Five gas-only models (1-5 in table 2.1) were used to test different disc gas masses and viscosity. A further two Phantom models were created using Phantom's "two-fluid" method (Price et al., 2018) to create discs containing dust grains that were sufficiently large that the dust and gas behave as two discrete fluids and their motion is decoupled (Price et al., 2018). This is due to the chosen dust grain sizes being large enough that the Stokes number is greater than unity. Under the "two-fluid" approximation, two different dust grain sizes were tested.

Model 2B (the fiducial model) was run twice, once for a much longer duration ($\sim$ 1150 years = 5 wide binary orbits) with the disc's outer edge was set to be larger than in all of the other models (6 AU rather than 4.6 AU) to study the long-term effects of interactions between the outer binary and the disc when the disc extends out further than the other models assume. This was then compared to past studies of the HD98800 system which also studied interactions between the disc and the outer binary (e.g. Smallwood et al., 2022), and the possibility of any effects caused by a wider disc being visible in the light curve discussed. However, for all subsequent models, including the second run of model 2B, the simulation duration was reduced and the disc radius set according to our estimates from Kennedy et al. (2019). This was done due to limitations on the availability of computational resources and the decision that any long-term effects on the disc caused by the orbit of the outer binary do not need to be studied in every simulation.

The wavelength chosen for radiative transfer modelling, $0.8\mu m$, was chosen since it corresponds to an optical colour band (I band) used by multiple observatories and has been used in past observations of circumstellar discs (e.g. Rodriguez et al., 2015). Since the goal is for the synthetic observations generated here to be comparable to real observations, it follows that a wavelength that the system can be observed at is used for modelling. This choice of wavelength also justified the assumption made for most simulations that the dust distribution follows the gas, since optical opacity is dominated by smaller dust grains which will be well-coupled to the gas ($St \sim 10^{-5}$).

Phantom models 1-5 (including the second run of model 2B) were run with all three sets of MCFOST parameters. Phantom models 6 and 7 already contained dust at a single, fixed dust mass prior to the radiative transfer step so only needed to be run for that single dust mass in MCFOST. In chapter 3, the results produced by comparing some of these models are presented and discussed.

Chapter 3

Results and Discussion

Once the grid of models described in section 2.5 had been run and the corresponding light curves, as well as the simplified `REBOUND` light curve created, the models and light curves were compared to assess what observable effect, if any, each free parameter had. In this section, I will begin by discussing the results from the N-body simulation, followed by general results from the fiducial simulation, then go through each set of models where a single parameter was changed and discuss what differences could be seen in their light curves, what this may tell us about the disc, and how this should inform future observations of the transit.

3.1 N-Body Simulation

Before looking at the hydrodynamical simulations, we can first consider the light curve generated using the `REBOUND` N-body simulation. Although this cannot tell us anything about disc properties, it can provide an idea of what we expect the general shape of the light curve to be and what key features we can expect to see.

Several key features can be highlighted on fig 3.1, as they relate to properties of the disc and stars:

1. Two distinct dips are visible, corresponding to the stars passing behind the lower and upper halves of the disc with an increase in flux observed as the stars pass behind the disc cavity.
2. Both Aa and Ab's light curves display an overall "V" shape (from ingress of the first dip to egress of the second dip), resulting from the assumption that optical depth is lower further from the stars.

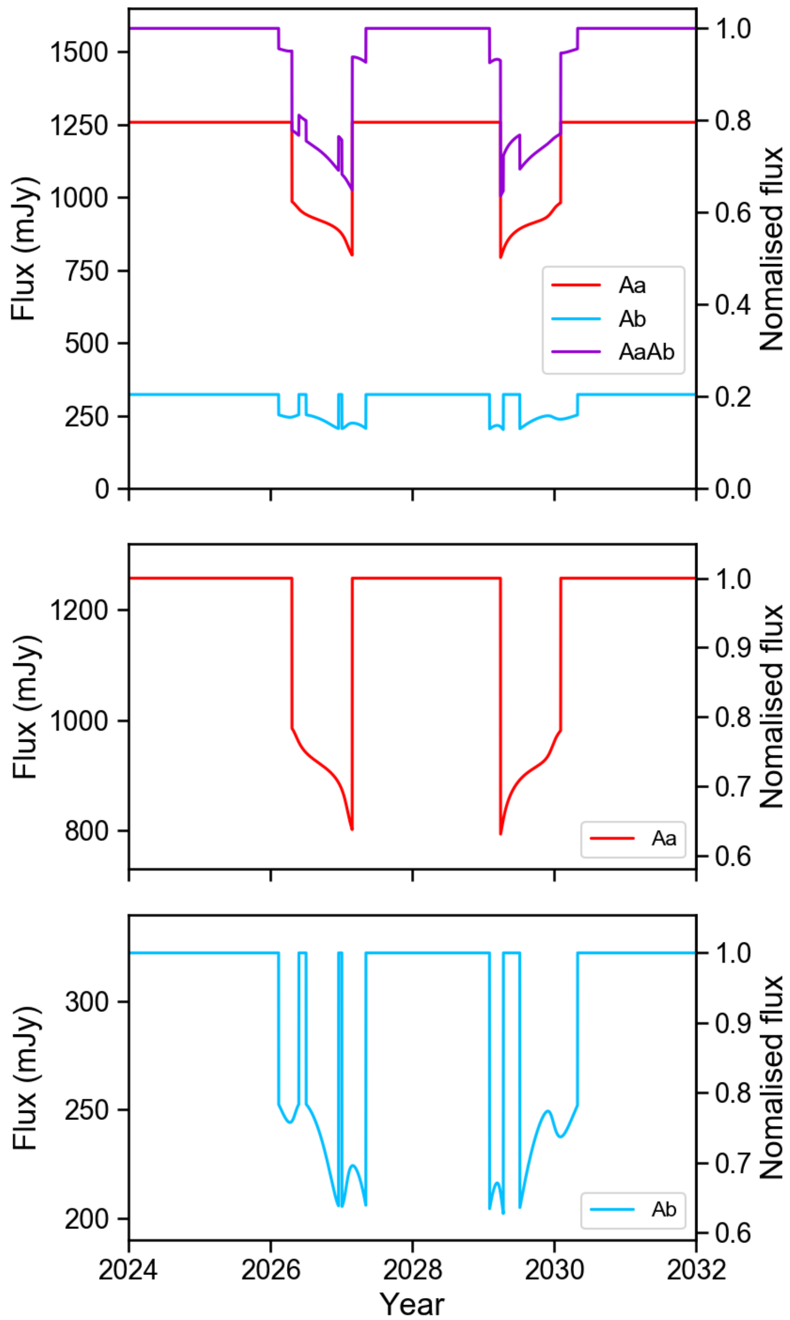

Figure 3.1: Light curves produced using `REBOUND` simulation data and an assumed static disc with a an optical depth profile $\tau \propto r_0/r$. Fluxes have been normalised using an Aa-Ab flux ratio of 3.9. The light curves show two distinct drops in flux, with the flux from Ab displaying more variation than the flux from Aa due to its "looping" motion close to the disc edges.

3. The light curve of Aa has a much smoother shape compared to the sharp variations in the light curve of Ab. This can be understood by looking at fig 2.1 - the lower mass of Ab means that it "enters" and "exits" the disc multiple times during the transit, leading to the features seen.

4. fig 3.1 indicates that the total light curve will be dominated by light and features from Aa, given that it is the brighter and more massive of the two stars.

Although the light curve produced via this method served as a useful preliminary result, offering some insight into the approximate shape and some key features we could expect to observe in light curves made from a more accurate model, the main shortcomings of this method should be noted. The first of these is that the disc's inner and outer edges have been imposed, based on empirical values from past observations, rather than developing through tidal interactions with the binaries. In reality, the disc material will be diffuse at the disc edges, creating smoother light curves, and the disc edges themselves may be at slightly different radii. The optical depth profile defined was chosen to be an arbitrary, simple profile that accounted for the expectation that the disc optical depth would decrease further from the disc's centre. Although this likely results in a light curve shape that approximately aligns with that of a more accurately modelled disc, the absolute values calculated for the resulting drop in flux do not reflect anything physical. The real disc may have an optical depth profile that is very different to this one, although we would expect some similarities, such as the inner edge of the disc being denser than the outer edge. It is also possible that the disc cavity will contain some material, so some variation in the light curve may be observed as the stars pass behind the cavity. This model also a assumes a perfectly static, azimuthally symmetric disc. However, the motion of the disc's material will likely have some observable effect on the light curve. For instance, it is possible that perturbations caused by the outer binary's motion around the disc could lead to non-axisymmetric features such as spiral arms forming at the disc's outer edge. Key effects such as tidal perturbations or accretion, cannot be studied using this simulation.

3.2 Hydrodynamical Simulations

In the following section, the results from the grid of models described in section 2.5 are discussed. Each light curve shown consists of the varying flux from Aa and

Ab, as well as the flux from BaBb, the value of which was interpolated from table 2 in Ribas et al. (2018) and assumed to be fixed over the course of all simulations. For each variable parameter, the models for which only that parameter was varied have been compared in turn, to attempt to discern any observable effects due to that single parameter. For each model, the approximate start and end dates of the transit have also been provided, defined by the earliest and latest dates when the flux drops below 95% of the maximum flux. Based on this, as well as the light curve features that are observed, some suggestions for future observations of the system and transit have been provided.

3.2.1 The Fiducial Simulation

The fiducial simulation (model 2B) was run twice, the first time with a slightly larger disc radius and for a much longer duration, with the shorter run serving as the baseline for all subsequent models with different parameters to be compared to. The light curve produced from the shorter run of this simulation can be seen in fig 3.2.

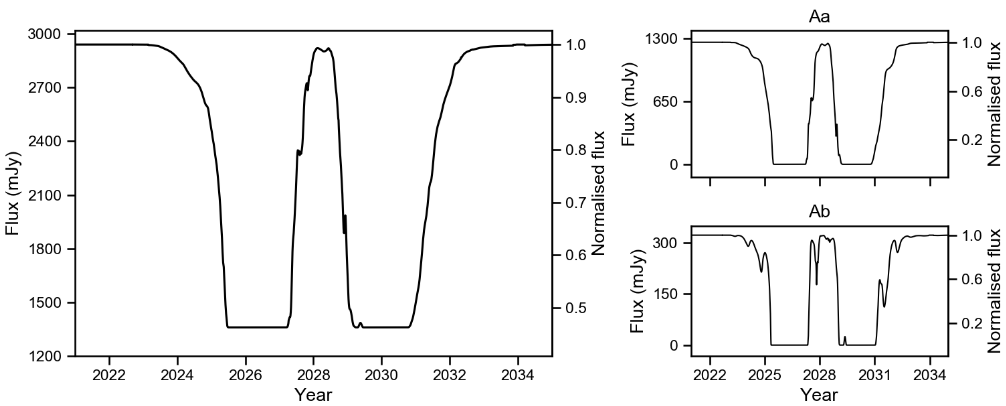

Figure 3.2: Left: Light curve for a system consisting of AaAb, BaBb and a disc with $M_{dust} = 0.33M_{\oplus}$, $M_{gas} = 33M_{\oplus}$, and $\alpha = 0.005$ at a wavelength of $0.8\mu m$ (model 2B). Right: Light curves showing the variation in flux received from the individual stars, Aa and Ab. The flux from BaBb (assumed to be constant) was not added here.

There are a number of similarities between this and the `REBOUND` light curve to note. The first of these is that two distinct dips are seen, with Aa contributing more strongly to the overall shape of the light curve than Ab. The motion of Ab behind the disc does lead to noticeable flux variations in the individual light curve for Ab, as Ab "loops" in and out of more optically thin regions over a relatively short period of time (as seen in fig 2.1). However, due to the flux of Ab being significantly less than that of Aa, this effect is not easily visible in the total light curve of the system. The shape of the dips is also similar to what was seen in the `REBOUND` light curves, with a gradual ingress of the first dip and egress of the second dip. However, the slope in the `Phantom` model is much steeper, since this disc was more realistically modelled to be optically thick, leading to the flux dropping to zero for the majority of the transit.

When allowed to run for longer with a larger radius, this simulation provided an opportunity to study the longer-term behaviour of the disc and its interactions with the outer binary, AaAb. It was found that a radius of 6 AU was large enough for the disc to be perturbed by the outer binary on each passage of AaAb around the disc, inducing spiral arms on the outer edge of the disc, as seen in fig 3.4. These perturbations began shortly after AaAb passed through the periastron, taking a few months to develop fully, and lasted long enough for their effects to be visible in the light curve of a transit. By the time AaAb had almost completed its orbit around BaBb and was approaching periastron again, the features would typically have begun to fade slightly. Upon AaAb reaching periastron, the features would begin to form again. None of the simulations with smaller discs displayed perturbations of this nature.

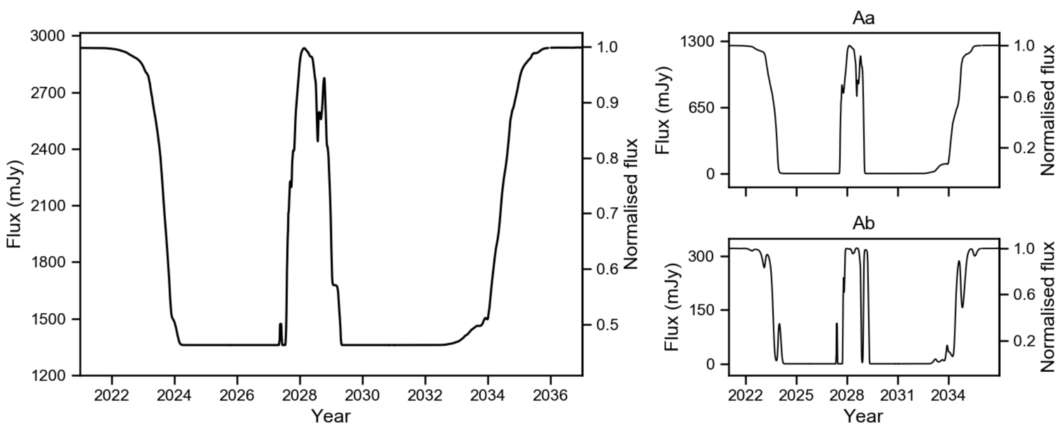

Figure 3.3: Left: Light curve for a system consisting of AaAb, BaBb and a disc with $M_{dust} = 0.33M_{\oplus}$, $M_{gas} = 33M_{\oplus}$, at a wavelength of $0.8\mu m$ (model 2B), run with a 6 AU disc for 5 wide binary orbits prior to the transit. Right: Light curves showing the variation in flux received from the individual stars, Aa and Ab. The flux from BaBb (assumed to be constant) was not added here.

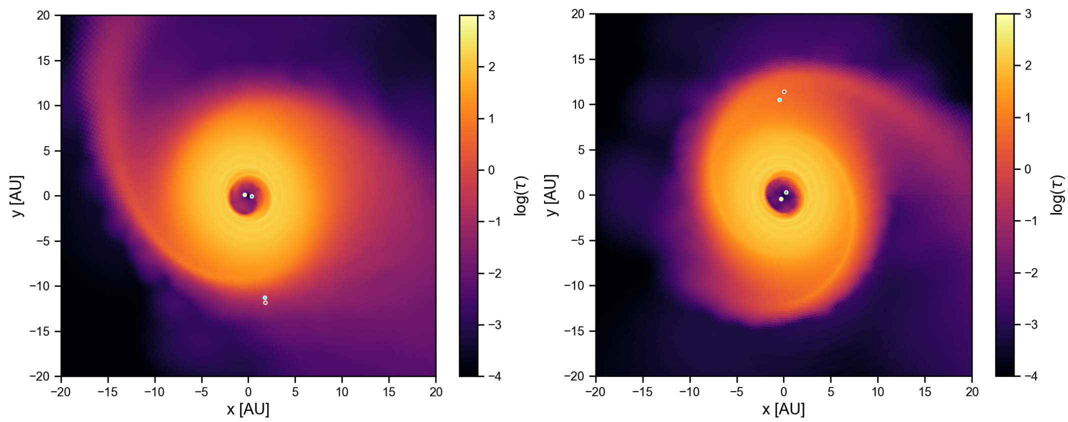

Figure 3.4: Snapshots of model 2B run with a larger disc radius, showing the spiral arms forming on the outer edge of the disc due to interactions with the outer binary. Left: 02-2023. Right: 06-2033. The positions of the stars are marked by coloured dots.

As can be seen in fig 3.3, the transit lasts longer for a 6 AU disc, in large part due to the excitation of spiral arms on the disc outer edge, caused by the proximity of AaAb as it passes close by the disc edge prior to the start of the transit. These arms, although less optically thick than the disc (see fig 3.4), are still optically thick enough to reduce the flux from AaAb to less than 10% of its incident flux, making the disc appear larger in the light curve. Because this excitation occurs just as the transit begins and it takes a few months for the features to form, the resultant effects are more visible in the second half of the transit, which is prolonged relative to the first due to the motion of the stars causing them to pass directly behind the spiral arms. This asymmetry of the light curve allows us to differentiate between this transit and the others discussed in this section, as any fixed properties of the disc, such as dust mass or viscosity, alter both halves of the transit in the same way, leading to an approximately symmetric light curve, while the excitation of spiral arms does not.

It is worth noting that as well as exciting spiral arms at the disc's outer edge, each periastron passage of AaAb also induced a change in the inclination of the disc. The evolution of the disc's inclination over time can be seen in fig 3.5. Over each wide binary orbit, the tilt was seen to change by around 3-4°, in agreement with the results obtained by Smallwood et al. (2022) from a similar, three-star simulation. Although changes to the disc's inclination are unlikely to be detectable in a light curve, they may be worth measuring during observations of the system, since the strength of this perturbation is likely related to the orbital parameters of the system and properties of the disc. The rate at which the inclination of the disc changes after the periastron passage of A is $\sim 0.04°$/year, so measurements can be taken much less frequently than is required for observing the transit.

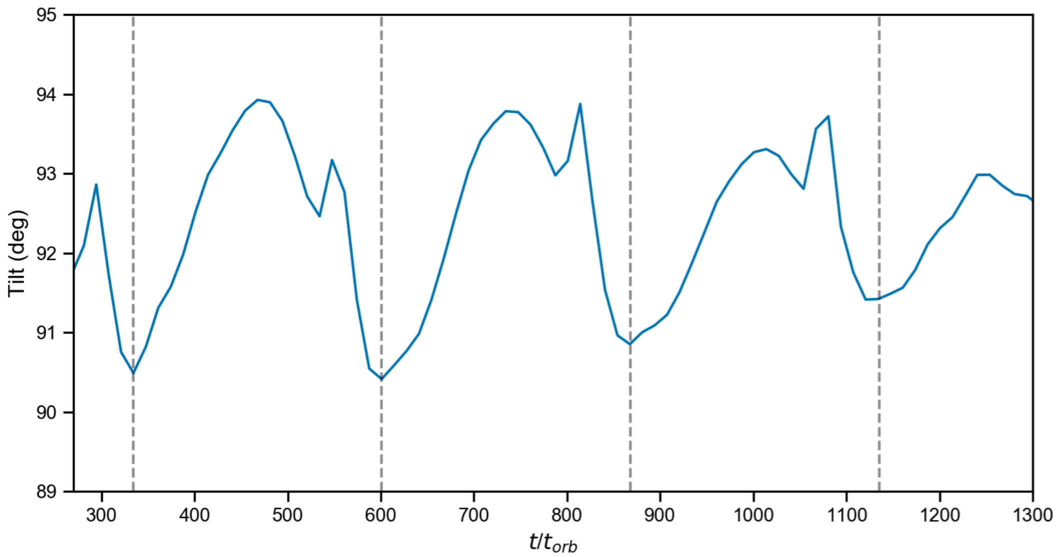

Figure 3.5: Tilt of the disc around BaBb over several hundred B binary orbits (model 2B, run with a 6 AU disc). The vertical dashed lines indicate the times when AaAb is at periastron.

3.2.2 Dust Mass

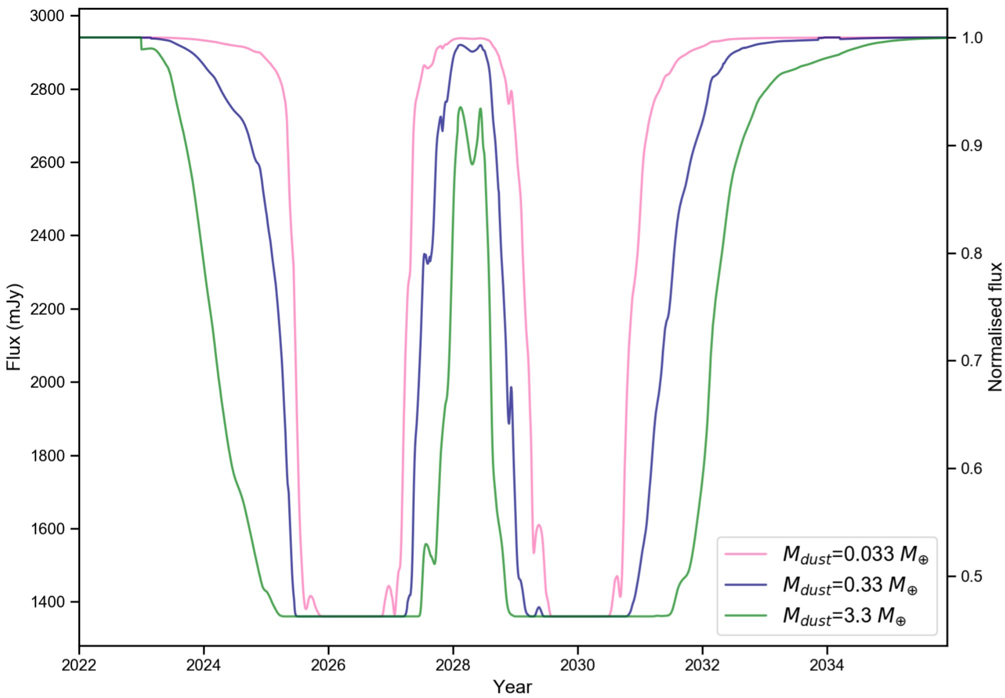

Figure 3.6: Light curves for discs with $M_{gas} = 33M_\oplus$, $\alpha = 0.005$, for the three tested dust masses, at a wavelength of $0.8\mu m$ (models 2A, 2B, and 2C).

The light curves for the three models tested with different dust masses are shown in fig 3.6. In general, a higher dust mass was found to correspond to higher optical depths throughout the disc, as expected. This led to an earlier drop in the flux at the disc edges and transits that appeared to begin sooner and end later, due to the higher dust mass disc being more optically thick, even at larger radii. As a result, the disc appears larger, due to being optically thick enough to block light from AaAb, even at the lower density regions at its outer edges. Due to the optical depth being non-zero throughout the disc cavity for an optically thick disc, some light curve features can be observed as stars Aa and Ab pass behind the cavity. The drop in flux can be caused by disc features internal to the cavity, such as spiral arms caused by perturbations by the inner binary. Most simulations showed some disc matter being pulled inwards to form spiral arms, though how visible such activity is in the corresponding light curves is dependent on the optical depth of those regions. Alternatively, some features can be due to the motion of the stars, as the `REBOUND` simulations have clearly shown that some short-term variations in flux are due to the stars moving in and out of more optically thick regions of the disc for a short

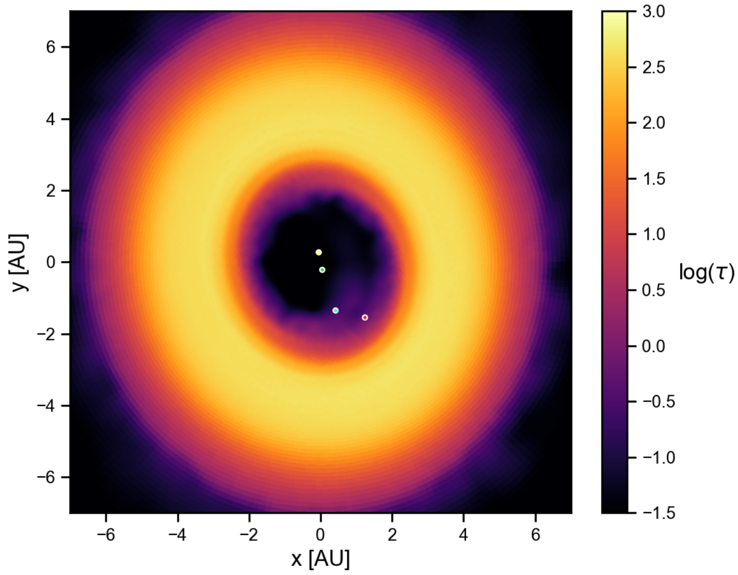

Figure 3.7: Optical depth map for model 2B, with a dust mass of $0.33 M_{\oplus}$, at a wavelength of 0.8 μm. This timestep corresponds to the features seen at around 2027.5 in fig 3.2 as the first transit ends. The limits for the optical depth have been manually set so the disc is deliberately over saturated, but some non-axisymmetric features inside the disc cavity can be seen, that are also present in the light curve in fig 3.6. The positions of the stars are marked by coloured dots. Red: Aa. Cyan: Ab. Green: Ba. Yellow: Bb.

duration (see figs 2.1 and 3.1). Studying snapshots from the simulations shows that the dip observed in the $M_{dust} = 3.3 M_{\oplus}$ model at around 2028.3, the midpoint of the stars' passage behind the disc cavity in fig 3.6 is an example of the latter – Aa and Ab briefly move closer to the disc inner edge, resulting in a slight drop in flux. However, the slight drop observed at 2027.5 in the $M_{dust} = 0.33 M_{\oplus}$ model, at the disc inner edge as the first transit ends, is due to the motion of lower density material inside the disc cavity, induced by the orbit of the B binary. This can be seen in fig 3.7. These features are seen once per inner binary orbit, and are typically accreted within a fraction of the inner binary period, so may or may not be easily detectable, depending on how optically thick these inner spirals are.

Given that these features exist in a lower density region of the disc, they are likely to be more noticeable if the disc is relatively optically thick in the cavity. However, for an optically thick disc, the period of the transit where the stars pass behind the disc cavity and their light is not completely obscured will be shorter, so observing such features will require observations to have a high enough cadence to allow for that. Some of the features seen in the light curves discussed here last as little as a 2-3 months and will require at least 10-20 data points to capture in sufficient detail, so taking measurements at least once a week would be ideal.

It is also worth considering how to distinguish between short-term features in the light curve caused by features of the disc rather than the movement of the stars behind the disc. Using the well-constrained stellar orbital parameters, the positions of the stars behind the disc can be calculated during the transit to determine whether a small feature such as a sharp dip or peak in the light curve is due to a physical feature in the disc or simply one or both of the stars briefly passing behind a much more or less optically thick region of the disc due to their trajectories.

3.2.3 Disc Viscosity

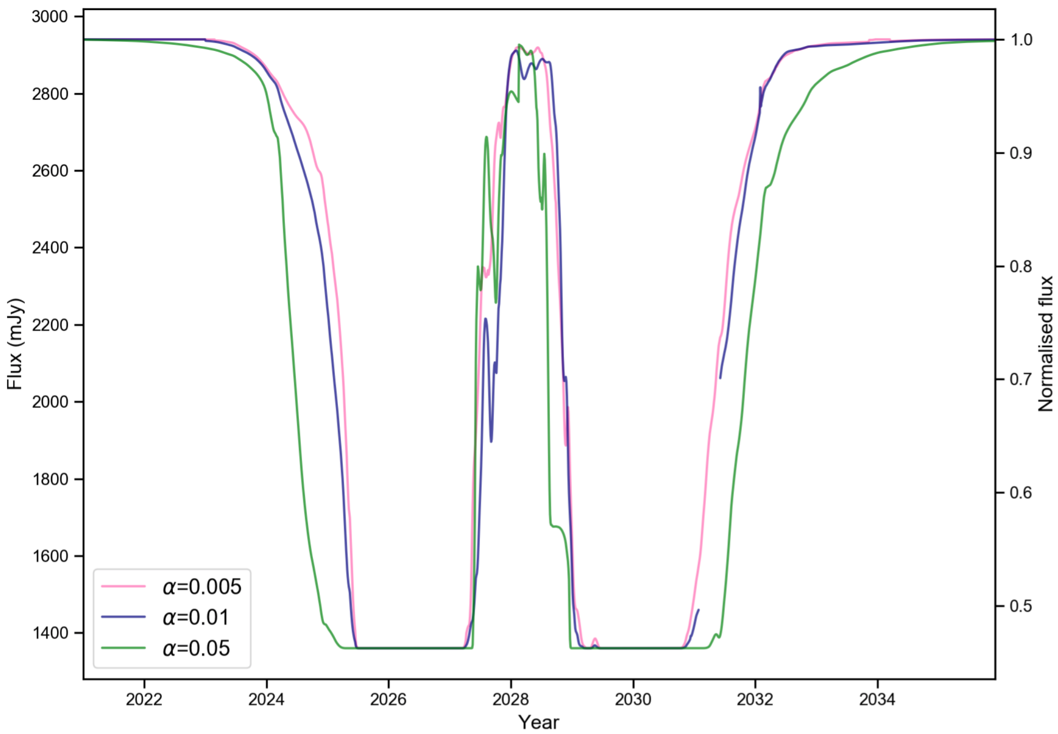

Figure 3.8: Light curves for discs with $M_{gas} = 33M_{\oplus}$, $M_{dust} = 0.33M_{\oplus}$, for the three tested values of α, at a wavelength of $0.8\mu m$ (models 2B, 4B and 5B). Due to computational issues, some data points are absent from the $\alpha = 0.01$ model.

The results in fig 3.8 show that the primary observable effect that a higher viscosity had on the shape of the light curves is that the dips caused by the transit are wider. However, unlike the widening of the transits caused by a higher dust mass, a higher viscosity caused the disc to be wider at the outer edges specifically. This aligns with our understanding of how viscosity affects disc dynamics - the disc's outer edge is set by the viscous spreading of the disc material (as well as interactions with outer companions), while the inner edge is primarily set by interactions with the inner binary. This is consistent with the fact that the cavity size is approximately the same across all three simulations with different α values.

In general, this leads to the light curves of higher viscosity discs displaying a more gradual drop to zero flux, due to the outer edges of the disc having spread further. For the highest viscosity model ($\alpha = 0.05$), the first reductions in flux can be seen as early as the start of 2023, as the stars begin to pass behind the low density, outermost regions of the disc. How quickly the flux drops i.e. the slope of the light curve at this early point in the transit increases with the disc viscosity. It is possible that measuring the slope of the light curve during this period could allow for the disc's viscosity to be estimated. However, these early drops in flux are low enough that they may not be detectable, as they correspond to a fractional drop in flux of less than 1%. It is also worth noting that interactions between the disc and the outer binary over several wide binary orbits, something not simulated here due to computational limitations, would likely truncate the outer edges of the disc. Realistically, it would not be set by viscous spreading alone. Nevertheless, we expect that a higher α will yield larger discs and longer transits.

3.2.4 Gas Mass

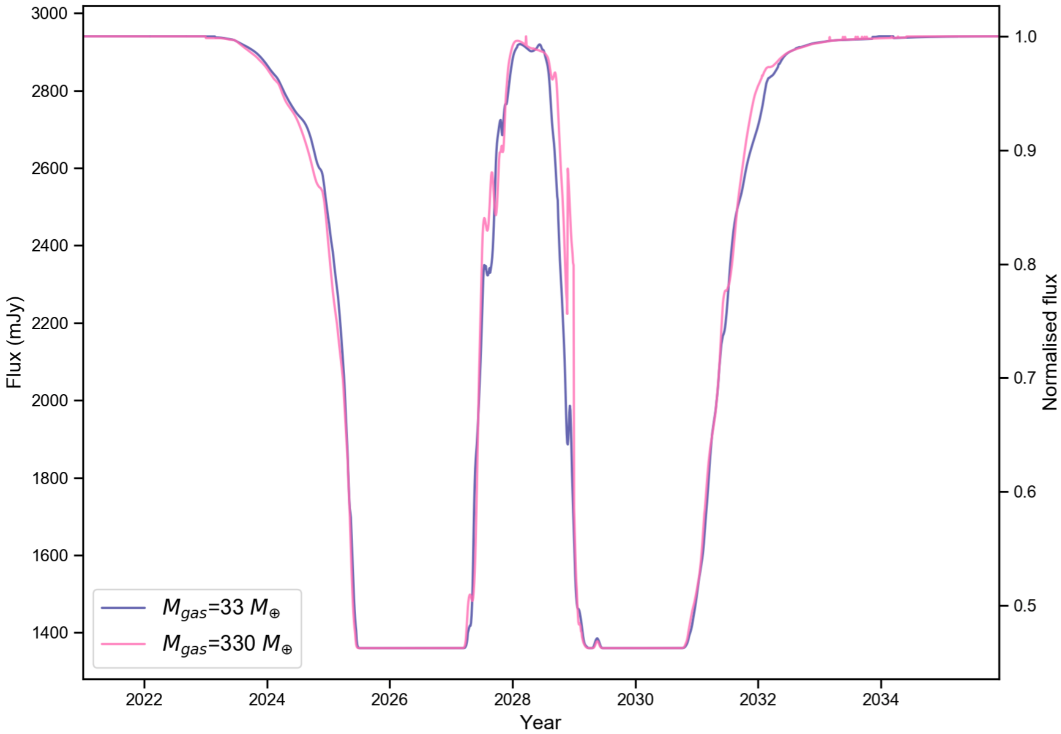

Figure 3.9: Light curves for discs with $M_{dust} = 0.33 M_\oplus$ and $\alpha = 0.005$ for the two of the three tested values of M_{gas}, at a wavelength of $0.8\mu m$ (models 2B and 3B). Due to computational issues with running `MCFOST`, light curves from only two of the three gas masses from table 2.1 have been presented here.

Fig 3.9 shows that changing the gas mass had a negligible effect on the the shape of the light curve and duration of the transit. This was an expected result, given that the dust mass in each of these models is the same, and is the primary source of the disc's opacity. However, it does mean that the light curve of the transit is unlikely to provide much information on the mass of the disc's gas component. Nevertheless, estimates of the disc's dust mass could be made using transit data and, assuming an approximate gas-dust ratio of 100, used to estimate the gas mass and compare it to values calculated from past observations of HD98800, based on the detection of gas tracers such as carbon monoxide (Kennedy et al., 2019).

3.2.5 Two-Fluid Simulations

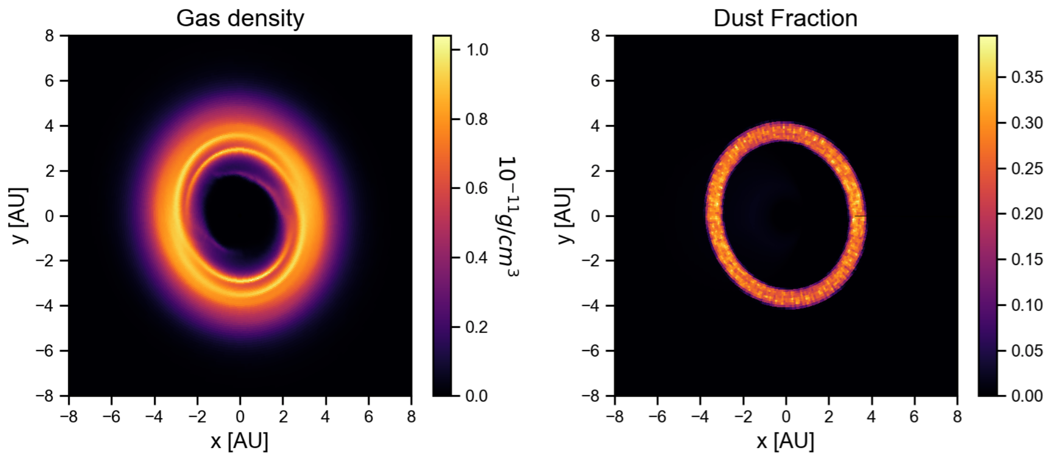

Figure 3.10: Comparison of the gas distribution vs. the dust distribution after 50 B binary orbits in a two-fluid simulation with 1cm dust grains.

Of the two models that were run using `Phantom` to simulate dust and gas, it was found that model 6, with 0.13cm sized dust grains, had not had enough time for the dust to reach a steady state radial profile by the end of the simulation so only model 7, with 1cm grains, is discussed here.

It was found that when dust grains are large enough that they are largely decoupled from the gas, the dust settles at radii that are within the gas extent, as seen in fig 3.10. In the model with 1cm sized dust grains, the dust ranged from around 3.1 to 4.2 AU, with the gas radius being around 2.5 to 4.6 AU . Realistically, the disc would have dust grains with a range of sizes, rather than one fixed size, and that size distribution is unknown. As a result, the radial extent the dust evolved to in this simulation differs from the values determined by Kennedy et al. (2019) from ALMA measurements which, with an observational wavelength of 1.3mm are more sensitive to mm sized grains than 1cm dust grains. However, this does confirm that the gas component may extend further than the dust, as noted by Kennedy et al. (2019). It also indicates that observations at longer wavelengths would likely show shorter transits, as they would be detecting larger dust grains with a smaller radial extent.

3.2.6 Timings for Observations

Table 3.1 contains the approximate dates for the four key points in the transit – the start of the first half of the transit, the end of the first half of the transit, the start of the second half of the transit, and the end of the second half of the transit. These were calculated by assuming a minimum 5% drop in flux was needed for the drop to be detectable (see fig 3.11) and hence, indicate the "start" (and end) of a portion of the transit. The blank cells on row 3 result from the fact that, for the highest dust mass model, the disc cavity was optically thick enough that the flux from the stars was below the 95% threshold throughout the entire duration of the transit.

It was found that having a higher dust mass or a higher α viscosity led to the transit beginning sooner and lasting longer. In general, the transit lasted around eight years, for a disc with gas and dust that are sufficiently coupled.

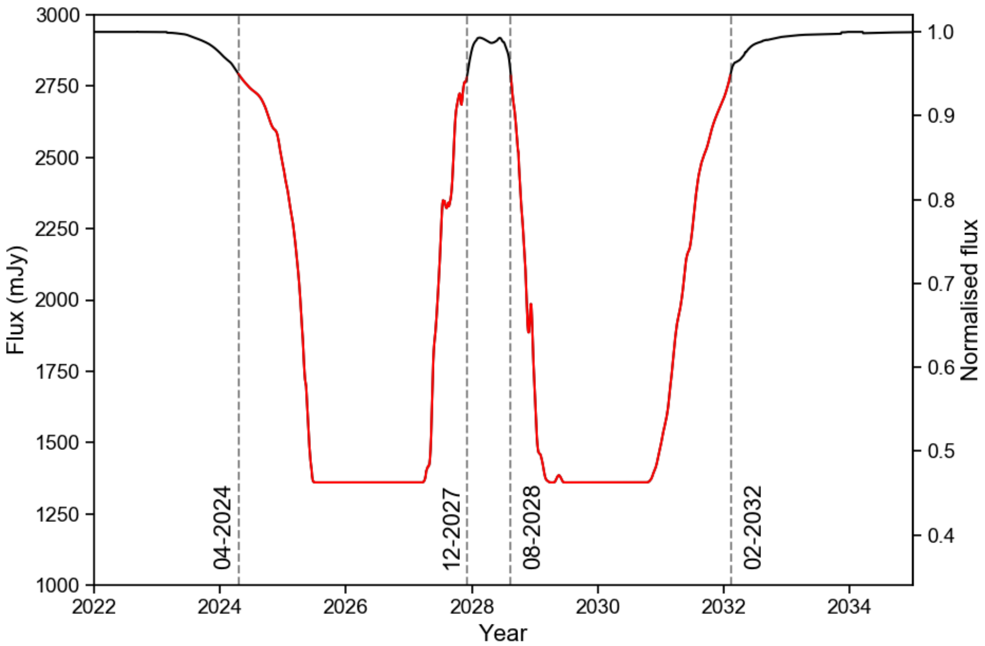

Figure 3.11: The light curve of the fiducial simulation (model 2B) with the four key dates indicated by the dashed vertical lines.

To estimate the required cadence for observations, the minimum detectable change in flux (assumed to be 5% of the maximum flux) was divided by the max-

Model	Dust Mass ($M_\oplus$)	Gas Mass($M_\oplus$)	α	t_1^{start}	t_1^{end}	t_2^{start}	t_2^{end}
2A	0.033	33	0.005	04-2025	05-2027	11-2028	04-2031
2B	0.33	33	0.005	04-2024	12-2027	08-2028	02-2032
2C	3.3	33	0.005	07-2023	-	-	12-2032
1B	0.33	3.3	0.005	12-2024	01-2028	07-2028	06-2032
3B	0.33	330	0.005	04-2024	11-2027	09-2028	12-2031
4B	0.33	33	0.01	03-2024	12-2027	09-2028	02-2032
5B	0.33	33	0.05	01-2024	02-2028	05-2028	11-2032
2B (longer run)	0.33	33	0.005	02-2023	12-2027	06-2028	01-2035

Table 3.1: Table of the approximate start and end dates of each of the two parts of the transit.

imum rate of change of flux dF/dt, estimated from fig 3.12. For all models with $\alpha = 0.005$, the minimum cadence required to detect a change in flux was approximately 6 days. For the highest viscosity ($\alpha = 0.05$) model, the minimum cadence required was approximately 2 days. However, both values corresponded to times when the stars were close to the inner or outer edge of the disc and the rate of change of flux was high. So although observing every few days when the the stars are close to any of the disc edges would be ideal, measurements can be taken much less frequently (for instance, once every 1-2 weeks) during the periods when the stars are completely obscured.

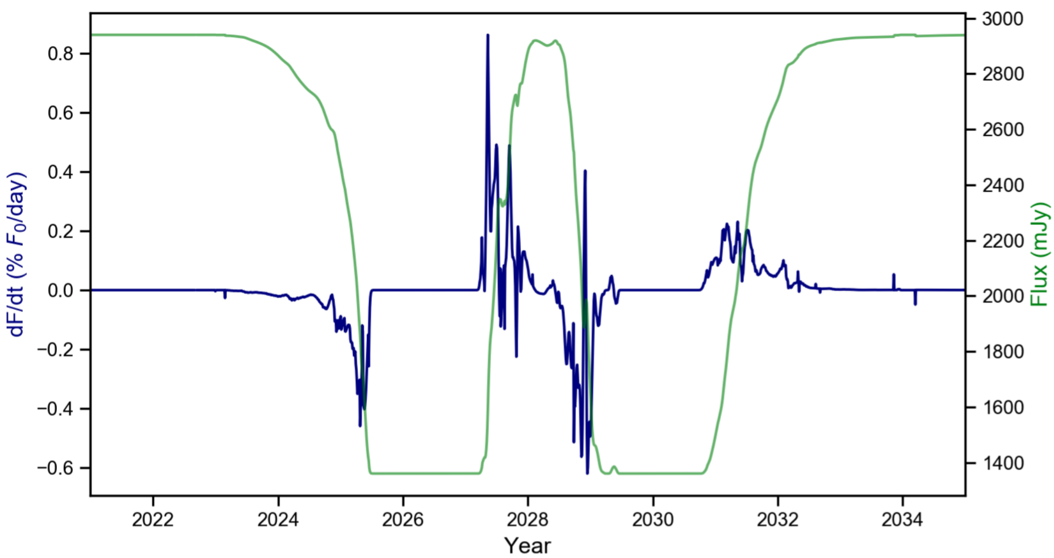

Figure 3.12: Light curve of the fiducial model (2B) plotted on top of the percentage rate of change of flux for that model. The percentage rate of change of flux for other models was also considered, and found to be comparable for all models.

3.2.7 Limitations

A number of limitations to these models should be considered when using them to inform further study of HD98800. The main one of these is that all but one of the simulations was run for a duration just long enough to allow for the disc to settle to a quasi-steady state and the transit to occur. However, the simulation that was run for a longer duration demonstrated that the outer binary does interact with the outer edge of the disc, although that effect may be less pronounced for a smaller disc. Any long-term effects and how they may be affected by the other tested parameters (viscosity, disc mass, etc.) have therefore not been studied here.

None of the simulations accounted for the growth and fragmentation of dust grains. Instead, the one-fluid simulations used a fixed dust grain size distribution, which was "painted on" to the model at each timestep, so did not evolve or redistribute itself with the simulation. The dust was also assumed to be well coupled to the gas in the optical depth maps. For an optical transit, small dust grains, which will be strongly coupled to the gas, are expected to dominate the opacity, so this would only slightly limit the accuracy of the modelling of dust grains in the one-fluid simulations. The two-fluid simulations used a single, fixed dust grain size, rather than a distribution of sizes, so were not ideal for considering how larger dust grains would realistically evolve in a disc with a range of grain sizes. All of these factors somewhat limited the accuracy of the modelling of dust grains in the simulations.

The models described here also omit any magnetohydrodynamic modelling, which would set the value of the α viscosity. Instead, this parameter was input manually. However, this is considered to be a minor limitation; the values chosen were justified by literature on the subject and the the modelling of discs with a chosen α is a well-established method for simulating accretion discs.

Chapter 4

Conclusion

4.1 Summary of Results

To conclude, this project focused on exploring some of the properties of circumbinary protoplanetary discs through the study of the circumbinary disc of one particular system, HD98800. Hydrodynamical modelling techniques were used to simulate a period where the disc of HD98800 will temporarily eclipse a pair of binary stars within the same system. I was able to compare synthetic observations and simulation data of this event across a grid of models and to existing observations of the system, in order to make inferences about certain properties of the disc.

It was found that the circumbinary disc of HD98800 is likely an optically thick disc, with a gas and dust component that have different radial extents. In some models, a spiralling motion of the disc material internal to the disc cavity was observed, which led to detectable features in the light curves of the transit. It was found that a greater dust mass resulted in a transit that lasted longer and saw a more immediate reduction in the flux. The disc cavity was also seen to be more optically thick in this case. More viscous discs had more diffuse outer edges, leading to a more gradual and early start to the transit, but had little effect on the disc cavity. A longer simulation that included the effect of the outer binary showed that the transit may be asymmetric due to the excitation of spiral arms when AaAb passes near the disc at periastron, assuming that the dust component extends out further than previous estimates have suggested.

These findings were used to provide two main sets of conclusions. The first being a set of key features to anticipate during observations of the real transit and what they may be indicative of. The second being suggested dates and cadences for observations, accounting for differences resulting from different disc parameters. This information could serve as beneficial to future observers of the system, as well as any further theoretical analysis of the transit.

4.2 Future Work

The research undertaken for this project was intended to inform future study of HD98800 and the transit. This particular system will only see this type of transit once every few hundred years, so ensuring that the upcoming transit is observed for the entire duration it occurs and at a cadence that will allow us to study the system in sufficient detail is crucial. According to the approximate start and end dates of the transit outlined in table 3.1, it would be ideal to begin observing the system from early 2023 until early 2033 at least, to ensure that the full transit is observed, even for a more optically thick, viscous disc. Some short-term features have also been seen in a number of light curves which are caused by the behaviour of disc matter inside the disc cavity. These would also be interesting to study, and tend to last for about 3 months. Ideally, the cadence of observations during this time should be high enough to allow for these features to be seen in observations - their duration, timings, and the fractional drop in flux they correspond to could all be measured and used to characterise the disc cavity.

If further research is to be done into this system prior to observations of the transit, it would be ideal to improve upon some of the limitations of the work presented here. The primary improvement that could be made would be for all of the simulations to be run for several orbits of the wide binary (as was done with model 2B only here). This would provide a more realistic model of the disc by allowing the disc to evolve under the effects of interactions between the disc and outer binary. Additional two-fluid simulations could be run of HD98800 that attempt to reproduce the dust and gas extents measured by Kennedy et al. (2019). This would require following the same method used to produce the two-fluid simulations discussed in section 3.2.5, but initialising the disc with different dust extents to determine which one evolves to a disc with the observed dust extent, studying how long this takes to occur, and what factors influence this evolution.

Time constraints did not allow for the generation and comparison of synthetic observations at different wavelengths but this would be a useful addition to the work presented here. Comparing observations in different filter bands would likely show reddening when the A stars are close to the disc's outer edge, as shorter wavelength light will be attenuated more. I would expect light curves to have the colour of only the B stars when A is completely obscured by the optically thick regions of the disc. This could provide some insight into how the disc should be observed. At shorter wavelengths (e.g. U or V band), any change in flux due to the distribution of small grains would be a larger proportion of the total flux, making it easier to observe. However, the total flux from the system, as well as the flux from Aa, would be greater at longer wavelengths (e.g. I band), making smaller variations easier to detect. In reality, HD98800 is fairly bright, being less than 50 pc away, so obtaining high signal-to-noise light curves across several bands should be relatively easy. Once the transit has been observed, returning to the results presented here for comparison may also provide some useful insight.

Appendix A

Access to Code and Data

A table showing a summary of the possible configurations that can be made using the `disc` module in `Phantom`:

Sinks	Disc Type	Disc Centre
1	circumstellar	origin
2	circumprimary	primary star
2	circumsecondary	secondary star
2	circumbinary	origin
3	circumtriple	origin
3	circumbinary	first hierarchical level secondary
4	circumbinary	first hierarchical level secondary

The shaded rows in the table indicate the two configurations added as part of this project.

The code can be accessed via https://github.com/amenafaruqi/phantom

Bibliography

Adams F.C., Lada C.J., and Shu F.H., 1987. Spectral Evolution of Young Stellar Objects, ApJ, 312:788. 4

Aly H., Lodato G., and Cazzoletti P., 2018. On the secular evolution of GG Tau a circumbinary disc: a misaligned disc scenario, MNRAS, 480(4):4738–4745. 7

Aly H. et al., 2015. Misaligned gas discs around eccentric black hole binaries and implications for the final-parsec problem, MNRAS, 449(1):65–76. 7

André P., 2015. In M. Gargaud, W.M. Irvine, R. Amils, I. Cleaves Henderson James (Jim), D.L. Pinti, J.C. Quintanilla, D. Rouan, T. Spohn, S. Tirard, and M. Viso, editors, *Encyclopedia of Astrobiology*, 2308–2313. 5

Andrews S.M., 2020. Observations of Protoplanetary Disk Structures, ARA&A, 58:483–528. 6

Armitage P.J., 2020. *Astrophysics of planet formation*. Cambridge University Press, 2nd edition. 3, 6, 7, 28

Artymowicz P. and Lubow S.H., 1994. Dynamics of Binary-Disk Interaction. I. Resonances and Disk Gap Sizes, ApJ, 421:651. 22

Artymowicz P. et al., 1991. The effect of an external disk on the orbital elements of a central binary, ApJ, 370:L35–L38. 6

Batalha N.M., 2014. Exploring exoplanet populations with nasa's kepler mission, *Proceedings of the National Academy of Sciences*, 111(35):12647–12654. 7

Bate M., Lodato G., and Pringle J., 2010. Chaotic star formation and the alignment of stellar rotation with disc and planetary orbital axes, MNRAS, 401(3):1505–1513. 7

Bate M.R., Bonnell I.A., and Bromm V., 2002. The formation of close binary systems by dynamical interactions and orbital decay, MNRAS, 336(3):705–713. iv, 2

Bate M.R., Bonnell I.A., and Price N.M., 1995. Modelling accretion in protobinary systems, MNRAS, 277(2):362–376. 19

Birnstiel T., Ormel C.W., and Dullemond C.P., 2011. Dust size distributions in coagulation/fragmentation equilibrium: numerical solutions and analytical fits, A&A, 525:A11. 5

Boden A.F. et al., 2005. Dynamical masses for low-mass pre-main-sequence stars: a preliminary physical orbit for HD 98800 B, ApJ, 635(1):442. 8, 11

Bohlin R.C., Savage B.D., and Drake J.F., 1978. A survey of interstellar H I from L alpha absorption measurements. II., ApJ, 224:132–142. 5, 29

Bonnell I.A. and Bate M.R., 1994. Massive circumbinary discs and the formation of multiple systems, MNRAS, 269(1):L45–L48. 3

Brennen C.E., 2009. *Fundamentals of Multiphase Flow*. Cambridge University Press. 5

Breslau A. et al., 2014. Sizes of protoplanetary discs after star-disc encounters, A&A, 565:A130. 7

Charbonneau D. et al., 1999. Detection of planetary transits across a sun-like star, ApJ, 529(1):L45. 7

Choudhuri A.R., 2018. *Astrophysics for physicists*. Cambridge University Press. 4

Clarke C.J. and Pringle J.E., 1993. Accretion disc response to a stellar fly-by, MNRAS, 261(1):190–202. 7

Dai Z. et al., 2021. In *Journal of Physics: Conference Series*, volume 2012, 012135. IOP Publishing. 7

Dohnanyi J., 1969. Collisional model of asteroids and their debris, J. Geophys. Res., 74(10):2531–2554. 5

Doyle L.R. et al., 2011. Kepler-16: A Transiting Circumbinary Planet, *Science*, 333(6049):1602. 1

Facchini S., Juhász A., and Lodato G., 2018. Signatures of broken protoplanetary discs in scattered light and in sub-millimetre observations, MNRAS, 473(4):4459–4475. 22

Franchini A., Lubow S.H., and Martin R.G., 2019. Circumbinary disk inner radius as a diagnostic for disk–binary misalignment, ApJ, 880(2):L18. 9, 21

Gaia Collaboration et al., 2022. Gaia Data Release 3: Stellar multiplicity, a teaser for the hidden treasure, *arXiv e-prints*, arXiv:2206.05595. 1

Gałan C. et al., 2012. International observational campaigns of the last two eclipses in EE Cephei: 2003 and 2008/9, A&A, 544:A53. 7, 8

Gingold R.A. and Monaghan J.J., 1977. Smoothed particle hydrodynamics: theory and application to non-spherical stars., MNRAS, 181:375–389. 18

Goodwin S.P., Whitworth A.P., and Ward-Thompson D., 2004. Simulating star formation in molecular cloud cores-I. the influence of low levels of turbulence on fragmentation and multiplicity, A&A, 414(2):633–650. 3

Haworth T.J. et al., 2018. Synthetic observations of star formation and the interstellar medium, New A Rev., 82:1–58. 13

Herschel W., 1782. Xii. catalogue of double stars, *Philosophical transactions of the Royal society of London*, (72):112–162. 1

Hirsh K. et al., 2020. On the cavity size in circumbinary discs, MNRAS, 498(2):2936–2947. ISSN 1365-2966. 6, 21, 22

Kennedy G.M. et al., 2019. A circumbinary protoplanetary disk in a polar configuration, *Nature Astronomy*, 3(3):230–235. 8, 9, 10, 12, 16, 17, 24, 28, 31, 43, 44, 49

Kennedy, Grant M, 2020. HD 98800. Available at `http://drgmk.com/sdb/seds/masters/sdb-v2-112205.29-244639.8/public/` [Accessed 20 June 2022]. v, 28

Kloppenborg B. et al., 2010. Infrared images of the transiting disk in the ε aurigae system, Nature, 464(7290):870–872. 7, 8

Kratter K.M., 2011. In *Evolution of Compact Binaries*, volume 447, 47. 3

Kraus A.L. et al., 2011. The role of multiplicity in disk evolution and planet formation, ApJ, 745(1):19. 1

Larson R.B., 2003. The physics of star formation, *Reports on Progress in Physics*, 66(10):1651. 5

Lubow S.H., Martin R.G., and Nixon C., 2015. Tidal Torques on Misaligned Disks in Binary Systems, ApJ, 800(2):96. 6, 22

Lucy L.B., 1977. A numerical approach to the testing of the fission hypothesis., AJ, 82:1013–1024. 18

Lynden-Bell D. and Pringle J.E., 1974. The evolution of viscous discs and the origin of the nebular variables., MNRAS, 168:603–637. 4

Martin R.G. and Lubow S.H., 2017. Polar alignment of a protoplanetary disk around an eccentric binary, ApJ, 835(2):L28. 7

Mathis J.S., Rumpl W., and Nordsieck K.H., 1977. The size distribution of interstellar grains., ApJ, 217:425–433. 6

Nixon C., King A., and Price D., 2013. Tearing up the disc: misaligned accretion on to a binary, MNRAS, 434(3):1946–1954. 7

Offner S.S. et al., 2010. The formation of low-mass binary star systems via turbulent fragmentation, ApJ, 725(2):1485. 3

Papaloizou J.C.B. and Nelson R.P., 2003. The interaction of a giant planet with a disc with MHD turbulence - I. The initial turbulent disc models, MNRAS, 339(4):983–992. 30

Penzlin A.B. et al., 2022. Binary orbital evolution driven by a circumbinary disc, A&A, 660:A101. 6

Pinte C., 2015. In *European Physical Journal Web of Conferences*, volume 102 of *European Physical Journal Web of Conferences*, 00006. v, 23

Pinte C. et al., 2006. Monte carlo radiative transfer in protoplanetary disks, A&A, 459(3):797–804. 23

Pinte C. et al., 2009. Benchmark problems for continuum radiative transfer-high optical depths, anisotropic scattering, and polarisation, A&A, 498(3):967–980. 23

Poon M., Zanazzi J., and Zhu W., 2021. Constraining the circumbinary disc tilt in the KH 15D system, MNRAS, 503(2):1599–1614. 8

Price D.J., 2007. SPLASH: An interactive visualisation tool for smoothed particle hydrodynamics simulations, PASA, 24(3):159–173. 24

Price D.J. et al., 2018. Phantom: A smoothed particle hydrodynamics and magnetohydrodynamics code for astrophysics, PASA, 35. 18, 31

Pringle J., 1991. The properties of external accretion discs, MNRAS, 248(4):754–759. 6

Rafikov R.R., 2017. Protoplanetary Disks as (Possibly) Viscous Disks, ApJ, 837(2):163. 30

Raghavan D. et al., 2010. A survey of stellar families: multiplicity of solar-type stars, ApJS, 190(1):1. 1

Ragusa E. et al., 2020. The evolution of large cavities and disc eccentricity in circumbinary discs, MNRAS, 499(3):3362–3380. 21, 22

Rein H. and Liu S.F., 2012. REBOUND: an open-source multi-purpose N-body code for collisional dynamics, A&A, 537:A128. 15

Rein H. and Spiegel D.S., 2015. IAS15: a fast, adaptive, high-order integrator for gravitational dynamics, accurate to machine precision over a billion orbits, MNRAS, 446(2):1424–1437. 15

Ribas Á . et al., 2018. Long-lived protoplanetary disks in multiple systems: The VLA view of HD 98800, ApJ, 865(1):77. 8, 12, 14, 26, 35

Rodriguez J.E. et al., 2015. V409 Tau as Another AA Tau: Photometric Observations of Stellar Occultations by the Circumstellar Disk, AJ, 150(1):32. 31

Rodriguez J.E. et al., 2016. An Extreme Analogue of ε Aurigae: An M-giant Eclipsed Every 69 Years by a Large Opaque Disk Surrounding a Small Hot Source, AJ, 151(5):123. 7, 8

Shakura N.I. and Sunyaev R.A., 1973. Black holes in binary systems. observational appearance., A&A, 24:337–355. 4

Smallwood J.L., Lubow S.H., and Martin R.G., 2022. Accretion on to a binary from a polar circumbinary disc, MNRAS, 514(1):1249–1257. 31, 37

Steinacker A. and Papaloizou J.C.B., 2002. Three-dimensional Magnetohydrodynamic Simulations of an Accretion Disk with Star-Disk Boundary Layer, ApJ, 571(1):413–428. 30

Thun D., Kley W., and Picogna G., 2017. Circumbinary discs: Numerical and physical behaviour, A&A, 604:A102. 1

Tohline J.E., 2002. The origin of binary stars, ARA&A, 40(1):349–385. 3

Tokovinin A., 2018. The Updated Multiple Star Catalog, ApJS, 235(1):6. iv, 19

Tokovinin A.A., 1999. The visual orbit of HD 98800, *Astronomy Letters*, 25(10):669–671. 11

Van Leeuwen F., 2007. Validation of the new hipparcos reduction, A&A, 474(2):653–664. 9

van Werkhoven T.I.M., Kenworthy M.A., and Mamajek E.E., 2014. Analysis of 1SWASP J140747.93-394542.6 eclipse fine-structure: hints of exomoons, MNRAS, 441(4):2845–2854. 7, 8

Wikipedia contributors, 2007. Wikimedia commons. Available at `https://commons.wikimedia.org/wiki/File:Orbit1.svg` [Accessed 05 June 2022]. iv, 3

Wyatt M.C. et al., 2015. Five steps in the evolution from protoplanetary to debris disk, Ap&SS, 357(2):1–20. 5

Zúñiga-Fernández S. et al., 2021. The HD 98800 quadruple pre-main sequence system-towards full orbital characterisation using long-baseline infrared interferometry, A&A, 655:A15. iii, 8, 9, 10, 11, 14, 15, 24